We are IntechOpen,
the world's leading publisher of Open Access books
Built by scientists, for scientists

4,800
Open access books available

122,000
International authors and editors

135M
Downloads

Our authors are among the

154
Countries delivered to

TOP 1%
most cited scientists

12.2%
Contributors from top 500 universities

CLARIVATE ANALYTICS

BOOK CITATION INDEX

INDEXED

WEB OF SCIENCE™

Selection of our books indexed in the Book Citation Index
in Web of Science™ Core Collection (BKCI)

Interested in publishing with us?
Contact book.department@intechopen.com

Numbers displayed above are based on latest data collected.
For more information visit www.intechopen.com

Physical and Technological Aspects of Processing High-Purity Refractory Metals

Vadim Glebovsky

Additional information is available at the end of the chapter

http://dx.doi.org/10.5772/59397

1. Introduction

The chapter presented is in some sense autobiographical. At one time during my experiments, I was faced with a huge obstacle: to get high-melting metals, namely, molybdenum, tungsten, and niobium, of very high purity. The high purity of refractory metals primarily means the low content of the two stubborn interstitials – carbon and oxygen. The presence of carbon and oxygen in polycrystalline metals melted by an electron beam in a vacuum often makes further plastic deformation of the metal difficult and unpredictable due to increased brittleness. In part, –what is clear is that there is a segregation of interstitial impurities at grain boundaries, which complicates plastic deformation. The literature on this subject points to a similar conclusion, with a universal solution: to eliminate effects of segregation. This path is well tested during the steelmaking through the introduction of deoxidants and modifiers, which include a variety of chemical elements, including carbon. Our objective is to obtain the "elemental" metal, in which impurities must not exceed a few tens of ppb. The question then arises: To what extent can these impurities be removed? Is it even possible to obtain the refractory metal with an extremely low content of carbon and oxygen? What is the mechanism of the removal of interstitial impurities? What analytical methods can control the removal processes with an adequate accuracy? It turned out that these questions, to a large extent, do not have a reliable answer. Moreover, experiments aimed at the solution of similar problems have been very inconsistent, so we have to carry out a detailed analysis of the main theoretical and experimental works on this topic. The analysis has been done, and the theoretical model of the behavior of carbon and oxygen in the vacuum annealing of solid refractory metals, as well as of the special case – of the interaction of these interstitials in the liquid refractory metals in vacuum – has been developed. Knowing the complicated behavior of carbon and oxygen in refractory metals, experiments are conducted using crucible-free melting methods – vacuum

INTECH
open science | open minds

levitation of small droplets (15–20 g) in a high-frequency electromagnetic field and electron beam zone melting with a floating zone of the molten metal. Both methods are non-contact in nature and have a high rate of convection of the melt, that is, the liquid metal in the both methods has no contact with any of the refractory material, and the volume of the liquid metal contains convective flows acting at a high rate. This makes it possible to perform experiments actually in the diffusion-less area when the equilibrium of the carbon–oxygen reaction in a bulk of the liquid droplet can be achieved in seconds. In addition, for controlling the oxygen and carbon, the highly sensitive methods of analysis (e.g., the fast neutron activation analysis of oxygen and deuterons for the analysis of carbon) have been used. All this make it possible to establish and prove that under certain conditions (mainly the adequate initial content of carbon and oxygen), as a result of the interaction, both impurities can be arbitrarily very low. This knowledge is used when performing the second task: obtaining ingots of high-purity molybdenum and tungsten. Technological options for obtaining massive ingots of high-purity unalloyed molybdenum and tungsten of the high technological plasticity during plastic deformation have been developed. The rolled products are obtained in the form of the thin sheets and foils of high quality. This chapter presents consistent data to give a reader an idea of the present study of the interaction of carbon and oxygen in refractory metals and the essence of the developed theoretical model. For solving the puzzle of low carbon and oxygen, the first half of this chapter can be utilized. At least, if a reader would like to solve puzzles, he can turn the reading of this Chapter, especially the first half of it, in a very entertaining lesson. A separate section is devoted to the experimental confirmation of the validity of the developed model using crucible-free methods of melting and highly sensitive methods for analyzing the content of impurities in the samples of both molybdenum and niobium. In the last section of the chapter, the experimental data are presented on the technological plasticity of large ingots of molybdenum and tungsten (up to hundreds of kilograms).

2. Theoretical and experimental aspects of obtaining pure refractory metals

2.1. Characteristics of gas-forming impurities removal

The removal of interstitial impurities dissolved in the metal, in the gas phase or vacuum, is a complex process consisting of the following elementary steps [1]:

1. Diffusion transition of impurities from the volume of metal to the surface layer: $A_{dis}^{v} \rightarrow A_{dis}^{s}$.

2. Transition of impurity atoms across the interface on the metal surface in the chemisorbed state: $A_{dis}^{s} \rightarrow A_{ads}$.

3. Recombination of adsorbed atoms (adatoms) with adsorbed particles (adparticles) coming to the surface of the metal or to the gas phase.

4. Desorption of adsorbed molecules or direct desorption of adatoms impurities in the gas phase or vacuum: $A_{ads} \rightarrow A_{gas}$ or $A_{ads} + B_{ads} (B_{gas}) \rightarrow AB_{gas}$. A kinetic analysis of the complex

heterogeneous process has been conducted on the basis of the system of equations obtained from the conservation of the particle number. Assuming that the exchange of the impurity atoms between the surface and the gas phase (vacuum) is carried out by the desorption and adsorption flows with densities J^a and J^d, and between the surface and the subsurface layer, by the flows with densities J^θ and J^s, we obtain:

$$\partial N / \partial t = D \nabla^2 N \tag{1}$$

$$dN^n\big|_s/dt = J^D\big|_s - J^{s\theta} \tag{2}$$

$$n / dt = -J^d + J^{s\theta} \tag{3}$$

where N is the bulk impurity content, $dN^n\big|_s$ the planar impurity content in the surface layer, n the impurity content of the adatoms on the surface, $J^{s\theta}$ the resultant flux density from the subsurface layer to the surface, $J^D\big|_s = -D\big/[v_a(\nabla N)_s]$ the diffusion flux density in the interface, D the diffusion coefficient of impurities, v_a the atomic volume of metal–matrix (the content of impurity atoms is expressed in atomic fractions).
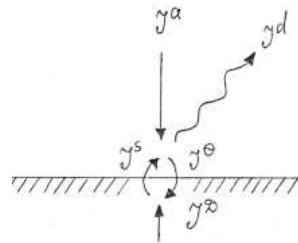
The system of equations can be solved only by numerical methods because of its complexity. The substantial simplification can be achieved on the basis of a quasi-stationary approxima-tion, according to which the impurity flows quickly adapt to each other so that the change in the content of impurities on the surface and in the subsurface layer is insignificant and can be neglected (a quasi-steady state). Assuming

$$J^D\big|_s - J^{s\theta} = dN^{\ddot{i}}\big|_s / dt \simeq 0; J^a - J^d + J^{s\theta} = dn / dt \simeq 0.$$

For two flux equations we write the matching condition of fluxes:

$$J^D\big|_s = \frac{-D}{v_a(\nabla N)_s} = J^{s\theta} = J^d - J^a. \tag{4}$$

Equalities (4) make it possible to formulate the boundary conditions within the framework of the adopted model to the diffusion equation (1) and determine them together with the boundary value problem. A solution to this problem allows the determination of the nature of changes in a local content of impurity atoms $N(\vec{r}, t)$, an average content of impurity atoms for a sample $N(t) > \int N(\vec{r}, t) dv$ and surface content of impurity atoms $n(t)$ in the course of their redistribution between the volume of metal, the surface, and the gas phase (vacuum).

2.2. Differences in energy state

Differences in the energy states of the impurity atom on the surface and in the metal lattice lead to an asymmetry of the potential relief in the vicinity of the interface (Figure 1). They lead to the well-known phenomenon of surface segregation of impurities [2-4]. Here, for a description of this phenomenon, reacting adatoms of impurities on the surface is usually neglected, and the surface energy is considered homogeneous. Within Langmuir approach for flux densities J^s and J^θ [5–8]:

$$J^s = v^s N\big|_s \left(1 - \theta\right) \tag{5}$$

$$J^\theta = \frac{1 - C_s}{v^\theta \theta} \tag{6}$$

where, $\theta = n / n_m$ is the degree of filling of the adsorption sites on the surface, $C = N/N_m$ the degree of filling positions in the solution implementation, v^s and v^θ the constants of the rate, which are proportional, respectively, to transition probabilities of impurity atoms from the subsurface layer to the surface and back. Thus, the flux density from the subsurface layer to the surface can be written as

$$J^{s\theta} = v^s N_s \left(1 - \theta\right) - v^\theta \theta \left(1 - C\big|_s\right), \tag{7}$$

or for the area of a dilute solution when $C\big|_s \ll 1$, $\theta \ll 1$

$$J^{s\theta} = v^s N\big|_s - v^\theta \theta. \tag{8}$$

An exchange of impurity atoms between the surface and the subsurface layer ($J^s \rightleftharpoons J^\theta$) occurs very rapidly, and at this stage of the quasi-equilibrium is established: $J^s \cong J^\theta \gg J^{s\theta}$.
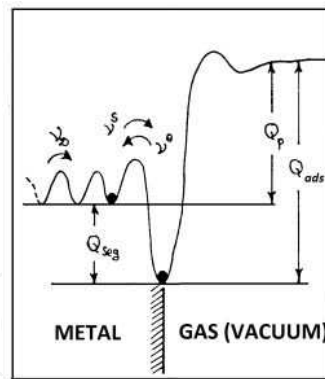
Note: Q_{seg} is the heat of segregation, Q_s the heat of dissolution, and Q_{ads} the heat of adsorption.

Figure 1. The potential relief for impurity atom in the vicinity of the metal–gas interface.

2.3. Adsorption and desorption phenomena on the surface of metals

Depending on the nature and strength of the bond of the adatoms and the admolecules the metal adsorption can be of two types: physical and chemical (chemisorption). In a state of physical adsorption, the adparticles hold on the metal surface by weak van der Waals forces and retain their individuality by having only a small perturbation of the metal. In this case, the physical adsorption heat is typically closer to the heat of molecular condensation and usually does not exceed 10 kcal mol^{-1}. In chemisorption the adparticles form strong chemical bonds (via an electronic exchange) with the metal surface, which in one way or another include covalent, ionic, or "metal" components and have been localized near certain active centers, distributed in accordance with the geometry of the surface structure of a solid metal. The heat of chemisorption is close to the heat of chemical reactions and often reaches several hundred kilocalories [9-12]. Typical lifetimes of adsorbed particles on the surface of a metal depending on their energy due to the metal can be estimated using the Frenkel equation [11]:

$$\tau = \tau_0 exp\left(Q / RT\right), \tag{9}$$

where τ_0 is the molecular vibration period equal to ~10^{-13} s; Q the heat of adsorption. Average lifetimes of adsorption of particles, calculated on the equation for certain values of Q and T, are shown in Table 1. It can be seen that a physically adsorbed film even at room temperature flies from the surface of the metal almost instantly, while the particles that are not strongly chemisorbed desorb even at temperatures above 1000 K.

A strong chemisorption is characteristic of interstitial impurities (hydrogen, oxygen, nitrogen, carbon), with a high "valence activity," which are adsorbed on the surface of transition refractory metals with relatively directed α-orbitals. By virtue of this, a direct desorption of the impurities is only noticeable at very high temperatures of the solid metal. In this case, in accordance with the first order reaction $A_{ads} \rightarrow A_{gas}$

| Binding energy Q, kcal.mole^{-1}	Average lifetimes of adparticles τ, s		Bond
300K	1000K		
<10	<10^{-6}	<10^{-11}	Physical adsorption
20	~30	~10^{-9}	Weak chemisorption
50	~10^{23}	~10^{-2}	Middle chemisorption
>100	>10^{60}	>10^{8}	Strong chemisorption

Table 1. Average lifetimes of adparticles calculated for certain values of the adsorption heat and temperature
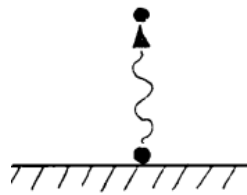
the desorption flux density is proportional to the content of adatoms [9,13]:

$$J_d = k_\alpha \theta \simeq n_m \theta / \tau, \qquad (10)$$

where n_m is the density of available adsorption sites, which is ~10^{15} at cm^{-2}. Despite the fact that the mechanism of the adatoms transition in the gas phase is the most simplest, it dominates by a relatively rare, as most energetically preferred, desorption processes of adatoms as a result of their recombination with other adsorbed particles presenting on the surface according with Langmuir-Hinshelwood mechanism, $A_{ads} + B_{ads} \rightarrow AB_{gas}$ (I) or as a result of their recombination with molecules impinging from the gas phase according with Ili-Ridil mechanism, $A_{ads} + B_{gas} \rightarrow AB_{gas}$ (II):
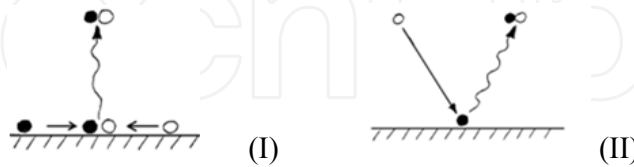
At the high vacuum annealing, the probability of an interaction with the molecules of the residual gas phase is relatively small, so the determining role belongs to the recombination processes by Langmuir mechanism (I). The energy required for breaking the bonds M–A_{ads} and M–B_{ads} (respectively Q_A and Q_B) is partly compensated by a heat release of the dissociation (D_{AB}) of AB_{gas} molecules ($A_{gas} + B_{gas} \rightarrow AB_{gas} + D_{AB}$). An effective activation energy, which at a weakly activated nature of the adsorption of molecules AB, is close to the heat of adsorption is: $E'_{d,AB} \simeq Q_{AB} = Q_A + Q_B - D_{AB}$. By comparing magnitudes of $E'_{d,AB}$ and Q_A the relatively simple

energy criterion can be achieved, according to which the desorption of adatoms A_{ads} by the reaction $A_{ads} + B_{ads} \rightarrow AB_{gas}$ would dominate their desorption in the atomic state in the case when the binding energy of the particles B with the metal is less than their binding energy in the molecule AB_{gas}:

$$Q_B < D_{AB} \tag{11}$$

In other words, the active partners of the recombination are only those particles that have a large enough "chemical affinity" with respect to the atoms of A and comparatively weak hold on the metal. In cases where the surface of the metal adatoms are only of one type A or there are relatively few active adsorption particles of any other type B, the direct desorption of adatoms can compete with two mechanisms, which are special cases of the process (I):

1. The pair recombination of adatoms of one type followed by the molecules desorption of simple diatomic gases $A_{ads}+A_{ads} \rightarrow A_{2gas}$ (III):
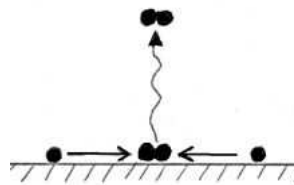
2. The formation and desorption of the compounds with the metal atoms of the substrate have the form M_nA_m, and in the simplest cases, MA: $A_{ads}+ M \rightarrow MA_v$ (IV).
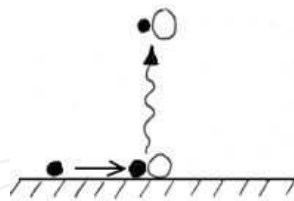
The condition (11) in the first case restricts the binding energy of the adatom–metal substrate [9]:

$$Q_A < D_{A2} \tag{12}$$

In a second case, the condition (11) limits an amount of the sublimation heat of the metal substrate (L_M) [14,15]:

$$L_M < D_{MA} \tag{13}$$

Thus, at a relatively weak bond of adatoms with the metal substrate ($Q_A < \min\{D_A, L_M - D_{MA} + D_{A2}\}$) the reversible selection of A_{ads} in the molecular state ($2A_{ads} \rightleftharpoons A2_{gas}$) dominates, and at a relatively weak coupling of $M–A_{ads}$ the irreversible selection of A_{ads} should prevail, or in the atomic state ($A_{2gas} \rightarrow 2A_{ads} \rightarrow 2A_{gas}$), if $L_M > D_{MA}$, or in the form of compounds with metal atoms of the substrate ($A_{2gas} \rightarrow 2A_{ads} \rightarrow 2MA_v$), if $L_M < D_{MA}$. Even if the explicit energy preference – the thermal desorption mechanisms comprising a step of the pair recombination – are implemented only when at their lifetime adparticles have enough time to overcome the distance separating them, that is, they have a sufficient mobility and before they are desorbed experience multiple mutual "collisions." The study of the surface diffusion using electron and ion projectors, as well as model calculations, show that the activation barrier, which must be overcome by diffusing particles to move from one center to the adjacent one, usually does not exceed 10–30% of the value of its binding energy Q. In other words, the potential relief of metal substrates is quite "smooth," so that even particles strongly chemisorbed on the surface rapidly migrate at relatively low temperatures [9, 16]. If the adfilm is rarefied and adparticles are randomly distributed among nodes of equivalent adsorption sites, forming an ideal lattice gas, the recombination rate is proportional to the concentration of recombining particles and can be written as:

$$J_R = k_R \theta_A \theta_B \,. \tag{14}$$

Here, $k_R = \mathrm{k_{R0}}\exp(-E_R/RT)$, and preexponential factor is typically rated as $k_{R0} \simeq (kT/n)n_m \approx 10^{28}$ at cm^{-2} s^{-1} [9, 13]. The resulting molecules, AB_{ads}, depending on the relative strength of the adsorption and intermolecular bonds can then, with a certain probability, dissociate again or can be desorbed into the gas phase. Therefore the total kinetic scheme of desorption of the dissociated phase ($A_{ads} + B_{ads}$) is as follows:

$$A_{ads} + B_{ads} \rightleftharpoons AB_{ads} \rightarrow AB_{gas} \tag{15}$$

The rate of dissociation and desorption of molecules AB_{ads} as first-order reactions, are given by:

$$J^D = k_D P_{00} \theta_{AB} , J^d = k_d Q_{AB} \tag{16}$$

Here, $k_D = k_{D0} \exp(-E_D/RT)$, $k_d = k_{d0}\exp(-E_d/RT)$, and $P_{00} \simeq (1 - \theta_A - \theta_B)^2$ is the probability of finding two unoccupied centers in the vicinity of the molecule AB_{ads}. In the steady state, when the fluxes of recombination J^R, dissociation J^D and desorption J^d are mutually balanced, that is, in the quasi-stationary approximation $J^R - J^D \simeq J^d$, then the total flux density of desorption of molecules AB is given by:

$$J^d = \Gamma^{\Theta}\Theta_A\Theta_B , \tag{17}$$

where $\Gamma_\theta = k_R k_d / (k_d + k_D) = \{k_R, k_d \gg k_D; k_R k_d / k_D, k_d \ll k_D\}$, the effective rate constant of desorption of AB from the rarefied ($P_{00} \to 1$) dissociated phase ($A_{ads} + B_{ads}$). In the limiting case $k_d \gg k_D$, the surface reaction $A_{ads} + B_{ads} \to AB_{ads}$ is practically irreversible, so that the process of the separation of molecules AB from the dissociated phase is controlled by the rate of recombination of A–B and is characterized by the effective activation energy of $E_d' \simeq ER \geq Q_{AB}$. In the opposite limit case $k_{d \ll} k_D$, the quasi-equilibrium $A_{ads} + B_{ads} \rightleftharpoons AB_{ads}$ is set in the adfilm. Against this quasi-equilibrium, the separation process of AB is controlled by the rate of desorption from the molecular state $A_{ads} \to AB_{gas}$ and characterized by the effective activation energy $E'_d = E_R - E_D + E_d = Q_{AB}$.

2.4. Thermal desorption of the metal–hydrogen and metal–nitrogen systems

Hydrogen and nitrogen, chemisorbed on the surface of the transition metals in the atomic state (dissociative), almost always are present in the gas phase in the molecular form (reversibly). The resulting pair recombination of adatoms H_{ads} or N_{ads} and the subsequent desorption of the weakly bound with the metal substrate molecules of H_2 and N_2 at kinetic reactions of the second order [13] is:

$$H_{ads} + H_{ads} \to H_{2\,gas} \tag{18}$$

$$N_{ads} + N_{ads} \to H_{2\,gas} \tag{19}$$

$$J_D = k^\theta \theta^2 \tag{20}$$

This is consistent with the energy criterion (12), according to which the dissociating diatomic adsorbate desorption occurs predominantly in the atomic state, if the binding energy of the adatom and the metal substrate Q exceeds the dissociation energy of the molecules in the gas phase D ($Q > D$) and in the molecular state in the case $Q < D$. Table 2 shows the binding energy of adatoms and the heat of chemisorption of hydrogen and nitrogen on an atomically clean surface of some transition metals. It is seen that values of Q_H and Q_N growing among Pt, Ir, Pd, Ni, Fe $\leq$ Re $<$ Mo $\leq$ W $<$ Nb $<$ Ta satisfy the inequalities:

$$Q_{H2} < Q_H < D_{H2} \tag{21}$$

$$Q_{N2} < Q_N < D_{N2} \tag{22}$$

Therefore, desorption of nitrogen and hydrogen in a molecular state is energetically advantageous process.

Metal	Hydrogen, D_{H2} = 103 kcal mol^{-1}		Nitrogen, D_{N2} = 225 kcal mol^{-1}	
	Q_{H2}, kcal mol^{-1}	Q_H, kcal g-at^{-1}	Q_{N2}, kcal mol^{-1}	Q_N, kcal g-at^{-1}
Tantalum	50	77	130-140	130
Niobium	-	-	120-130	175
Tungsten	33	68	80-85	155
Molybdenum	30	65	80-85	155
Rhenium	-	-	60-70	145
Iron, Nickel, Palladium, Iridium, Platinum	10-30	50-65	35-55	130-140

Table 2. The binding energy and heat chemisorbtion of hydrogen and nitrogen on atomically clean surface of transition metals

2.5. Thermal desorption of the metal–oxygen systems

In contrast to the reversible hydrogen and nitrogen, the evolution of molecular oxygen ($2O_{ads} \rightarrow O_{2\ ads} \rightarrow O_{2\ gas}$) is observed only in some precious metals, which is characterized by a relatively low binding energy of the oxygen adatoms with the metal substrate $Q_O < D_{O2}$ = 118 kcal mol^{-1} [17]. On the most transition and, in particular, refractory metals oxygen chemisorbs with relatively high binding energies $Q_O > D_{O2}$ (Table 3).

| Metals	Q_{O2}, kcal-mol	Q_O, kcal g-at^{-1}	Q_O, kcal g-at^{-1}
	Calorimetry		Mass-spectrometry
Titanium	238	178	-
Tantalum	214	166	179
Niobium	210	164	168
Tungsten	196	157	140
Molybdenum	173	146	-
Rhenium	-	-	127

Table 3. Binding energy of adatoms and heat of chemisorption of oxygen molecules

The basic mechanisms of the oxygen removal depending on the nature of the metal substrate are:
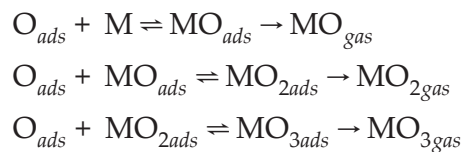
1. The direct desorption of oxygen adatoms in the atomic state $O_{ads} \rightarrow O_{gas}$.

2. The formation and desorption of metal oxides of the different stoichiometry $M+nO_{ads} \rightarrow MO_{n\ gas}$.

Data on the composition of the particles desorbed from the surface of refractory metals of Groups 4–7 after the oxygen chemisorption [14] are shown in Table 4. At low degrees of filling,

oxygen desorbs, or in the atomic state, or in the form of monoxide MO. Wherein the first type (I) of desorption ($O_{ads} \rightarrow O_{gas}$) is observed in metals of Groups 6 and 7 (molybdenum, tungsten, rhenium) with the low-volume oxygen solubility, the second type (II) of desorption ($M + O_{ads} \rightarrow MO_{gas}$) in metals of Groups 4 and 5 (zirconium, vanadium, niobium, tantalum) is characterized by high-volume oxygen solubility. In both the cases, the high-temperature desorption of oxygen from the rarefied adsorbed film proceeds as the first-order reaction:
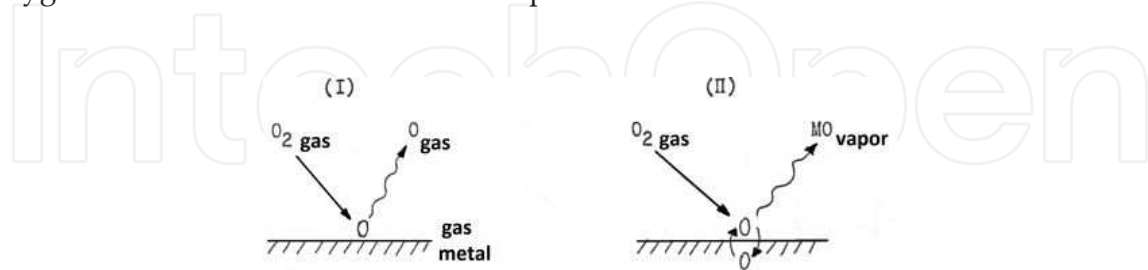
With an increasing degree of filling, the contribution of flows of polyoxygen molecules MO_A and MO_3 rapidly grow, and become predominant in the monolayer coatings $\theta \approx 1$. According to a generalized model of the interaction of oxygen with the transition metals [14, 15], and later confirmed by experiments for the systems of tungsten–oxygen, rhenium–oxygen, molybdenum–oxygen, niobium–oxygen, and tantalum–oxygen, that the formation of oxides proceeds in several successive stages, each of which is in the quasi-equilibrium. A limiting stage of the transition of oxygen into the gas phase consisting of oxides MO, MO_2 and MO_5 is their desorption:

$$O_{ads} + M \rightleftharpoons MO_{ads} \rightarrow MO_{gas}$$
$$O_{ads} + MO_{ads} \rightleftharpoons MO_{2ads} \rightarrow MO_{2gas}$$
$$O_{ads} + MO_{2ads} \rightleftharpoons MO_{3ads} \rightarrow MO_{3gas}$$

The effective activation energy $E'_{d,MO}$ of oxygen releasing from the atomic phase in the composition as oxides MO_n is expressed by

$$E'_{d,MOn} = nQ_0 - L_M + D_{MOn}$$

where L_M is the heat of the metal sublimation, D_{MOn} - MO_n the oxide dissociation energy in the gas phase ($MO_n \rightarrow M_{gas} + nO_{gas}$). Depending on the sign of the difference D_{MO} - L_M (the values of D_{MO} - L_M are given in Table 4), the value $E'_{d,MO}$ is more or less Q_0. Consistent with the simple energy criteria set out above, rhenium, molybdenum, and tungsten emit predominantly the atomic oxygen characterized by values $L_M > D_{MO}$, whereas titanium, zirconium, vanadium, niobium, and tantalum emit predominantly monoxides characterized by $L_M < D_{MO}$

On the basis of data on the oxygen solubility and the oxides desorption during the vacuum metal processing, the possibility of the oxygen removal (deoxidation) is evaluated by an evaporation ratio that is meaningful of the relation of the saturated vapor pressures of the

Metal	Desorbing particles		Temperature of the desorption start, K	D_{MO} - L_M, Kcal mol^{-1}	Maximal solubility of oxygen in metal, at.%
	$\theta \ll 1$	$\theta \approx 1$			
Titanium	TiO	TiO$_2$	-	44	32
Zirconium	ZrO	ZrO$_2$	>1900	36	30
Vanadium	VO	-	>1800	25	15
Niobium	NbO	NbO$_2$	>1900	7	11
Tantalum	TaO	TaO$_2$	>2100	7	8
Molybdenum	O(Mo)	MoO$_2$, MoO$_3$	>1700	-41	0.15
Tungsten	O	WO$_2$, WO$_3$	>1700	-46	0.06
Rhenium	O	(ReO$_2$) ReO$_3$	>1300	-47	0.01

Table 4. Composition of desorbing particles from the surface of refractory metals [14]

gaseous oxides and the metal over the metal surface in a vacuum, for the temperature interval 1800–2000 K (for which there are experimentally validated thermodynamic data) [18]. A serious disadvantage of this assessment is that it does not take into account the possibility of the high atomic oxygen desorption from molybdenum and tungsten. In any case, the currently available information concerning the thermal oxygen desorption from refractory metals reveals the following: Group 4 metals (titanium, zirconium, hafnium) have the greater oxygen solubility, the increased affinity for oxygen and the desorption of oxygen from these metals is in the form of oxides (monooxides); wherein the evaporation ratio is about 2–3, and the possibility of the oxygen removal from these metals due to desorption is extremely small. Titanium at $T > T_m$ is also poor due to evaporative deoxidation, but in the case of melting zirconium and hafnium it is possible to achieve a certain purification of oxygen. From Group 5 of metals (vanadium, niobium, tantalum), oxygen desorbs in the form of monooxides (suboxides) and the evaporation ratio is 28–42, that is, purification of these metals from oxygen by the monoxide desorption due to high-temperature annealing in vacuum is possible. The possibility of evaporative deoxidation in a more simplified form was shown by Ono and Moriyama [18] and Kulikov [19]. All common industrial metals were divided into three groups according to their capacity for "self-deoxidation" (Table 5). Note that in those studies the possibility of removing oxygen from molybdenum and tungsten in the atomic state has not been considered.

In the assessment [19] carried out for molten niobium and tantalum in vacuum, the evaporation ratio reaches 2,000–3,000, indicating intensive removal of oxygen from liquid metals of Group 5 in vacuum. In this case, the potential of the deep refining of tantalum at $T > T_m$ is much higher than that of niobium. An exception in this group is the system of vanadium–oxygen, which prevails in the vapor pressure of vanadium and, respectively, the evaporation rate is only about 4. By the thermodynamic assessment, the vapor pressure of gaseous vanadium oxides VO and VO$_2$ at $T > T_m$ is well below the saturated vapor pressure of vanadium over the melt. Therefore, evaporative deoxidation of liquid vanadium unlikely. The situation is similar to the case of

Evaporative deoxidation is possible	Evaporative deoxidation is impossible
MoO/Mo = $10^{0.5}$	Ti/TiO = 10
NbO/Nb = 10	V/VO = 10^2
BO/B = 10^2	Be/BeO = 10^3
WO/W = 10^2	Cr/CrO = 10^4
ZrO/Zr = 10^2	Mn/MnO = 10^5
ThO/Th = 10^3	Fe/FeO = 10^6
HfO/Hf = 10^4	Ni/NiO = 10^7
TaO/Ta = 10^4	

Table 5. Capacity of refractory metals for evaporative deoxidation

chromium. However, tungsten and molybdenum, other members of Group 6, are character-ized by the small oxygen solubility, by the low activity of dissolved oxygen, and by extremely high coefficients of evaporation, indicating a strong tendency of these metals to oxygen removal by the evaporation of oxides (oxygen). The major oxides are desorbed molecules like MO_3 and their dimers. At low content of oxygen in liquid molybdenum and tungsten at $T > T_m$ the oxygen should generally be present above the melt in the atomic state and the gaseous oxides desorption is negligible. The thermodynamic evaluation showed that at the removal of the diffusion supply of oxygen from the bulk of the liquid metal to the surface, from which desorption occurs, the deep removal of oxygen can apparently be achieved as a result of the vacuum treatment of liquid molybdenum and tungsten. The simple qualitative assessment of the high-temperature behavior of the metal–oxygen system in vacuum (and accordingly, the high-temperature metal processing, such as annealing and exposure in the molten state for the purpose of oxygen removal) can be divided into three types. In the first type (titanium, vanadium, chromium) oxygen desorption (or oxides) does not occur because the oxygen is strongly associated with the metal lattice and has the high thermo-chemical stability, and the metal itself has the vapor pressure greater than the vapor pressures of any oxides formed in this system. In the second type (molybdenum, tungsten), the vapor pressure of the oxides is much higher than the metal vapor pressure. In this case, the oxygen chemisorbed is easily desorbed alone or reacts rapidly with the metal and forms oxides, which are desorbed. The oxygen does not even dissolve in the metal lattice. The third type (niobium, tantalum, zirconium, and hafnium) is an intermediate between the first two.

2.6. Thermal desorption of the metal–carbon–oxygen

We have already noted that carbon is very strongly retained on the surface of metals and, unlike nitrogen and hydrogen, cannot be desorbed "independently" even from the surface of molten metal. The main mechanism of carbon release during vacuum annealing is the formation and desorption of CO molecules as a result of pair recombination of carbon and oxygen adatoms by the reaction [17]

$$C_{ads} + O_{ads} \rightleftharpoons CO_{ads} \rightarrow CO_{gas}$$
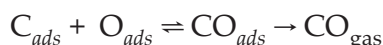
At sufficiently high temperatures of the metal substrate and the low contents of adsorbed particles when the adatom phase can be considered [20] as a two-dimensional gas (C_{ads} + O_{ads}), the resulting flux density of the CO desorption is given by $J^d = \Gamma^\theta \theta_o \theta_o$, where $\Gamma^\theta = (k_R k_d / k_D) \sigma$ is the effective constant of the CO desorption rate from the dissociated phase (C_{ads} + O_{ads}) and $\sigma = (1+k_d/k_D)^{-1}$ the probability of dissociation of the chemisorbed molecules CO_{ads}. In the limiting case $k_d \gg k_D$ ($\sigma \rightarrow 0$), practically all the formed molecules (CO_{ads}) are desorbed into the gas phase, so CO removal is controlled by the rate of recombination of the adatoms C_{ads} and O_{ads} and characterized by an effective activation energy $E'_d \simeq E_R$. In the opposite limit $k_d \ll k_D$ ($\sigma \rightarrow$ 1), the quasi-equilibrium C_{ads} + $O_{ads} \rightleftharpoons CO_{gas}$ is established in the adfilm, so the process is controlled by the release rate of the CO desorption from the molecular state and is characterized by the effective activation energy $E'_d \simeq E_R + E_d - E_D$. The question is which of these mechanisms is realized on the surface of the transition metals. It is closely linked to the question of the strength and character of the CO bond with the metal substrate [9, 21]. It is found that unlike molecular hydrogen, nitrogen and oxygen, the molecules of CO are firmly chemisorbed on the surface of transition metals to form the so-called β-structure state with one of the following types: (a) the bridge structure 2M-CO, and the CO molecular axis is perpendicular to the metal surface, and (b) the structure of the two-point adsorption of M-C-O-M, wherein the axis of the CO molecule is parallel to the metal surface.

(а)   (б)
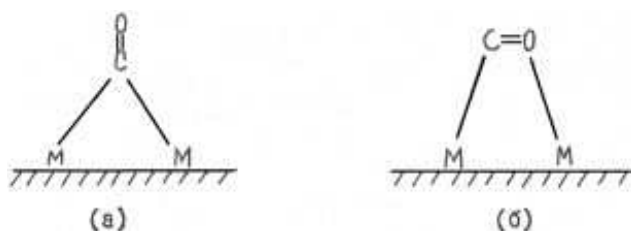
Already in the early studies, it is found that, despite the obvious weakening of the intramolecular bond of C–O, the β-chemisorbed molecules of CO on many transition metals have a high stability and do not dissociate substantially during the chemisorption process. For a long time this was considered to be the molecular nature of the chemisorption of CO on transition metals, as opposed to the distinct dissociative chemisorption of hydrogen, nitrogen, and oxygen. Recently it has been shown [22] that, depending on the nature of the metal and the heat of chemisorption Q_{CO}, the β-chemisorption of CO can be of both molecular and dissociative character clearly. It is assumed that there exists a critical value of the chemisorption heat ($Q_{CO} \geq 65$ kcal mol^{-1}), from which the CO molecules show a tendency to dissociation. Table 6 presents the calorimetric data on the initial heats of the CO chemisorption on films of certain transition metals [21] specifying the nature of the chemisorption observed in each case.

The CO chemisorption on transition metals (platinum, palladium, rhodium, iron, nickel, cobalt, etc.) of Group 8 and rhenium of Group 7 is relatively weak ($Q_{CO} \leq 60$ kcal mol^{-1}). So, the CO molecules on the surface of these metals are sufficiently stable and hardly dissociate due

Metal	Q_{CO}, kcal mol^{-1}	Chemisorption mode
Titanium	155	
Zirconium	150	Dissociative chemisorption with dissolving in metal lattice
Niobium	123	
Tantalum*	110	
Tungsten	85-90	Dissociative chemisorption (?)
Molybdenum	70-80	
Rhenium*	62	
Platinum	50	
Cobalt	48	
Rhodium	47	Molecular chemisorption
Iron	45	
Palladium	43	
Nickel	42	

*Q_{CO} for Tantalum, Rhenium were received by flashing

Table 6. Initial heat and character of chemisorbtion of CO on some transition metals [21]

to moderate temperatures and the presence of high energy barrier to dissociation of CO, the value of which exceeds the binding energy of CO–metal [16, 22]. When the metal substrate is rapidly heated to the high temperature (flashing), the entire β-CO layer chemisorbed at room temperature has enough time to be desorbed before the dissociation rate becomes significant. The thermodesorption process obeys first order kinetics, i.e., it is molecular [9, 21, 23]. Refractory metals of Group 6 (tungsten and molybdenum) chemosorb CO quite strongly ($Q_{CO} \simeq 70 \div 90$ kcal mol^{-1}), so the dissociation probability of the CO molecules on the surface of these metals, apparently, is significantly higher than in the previous case, although the nature of the CO chemisorption on tungsten and molybdenum is still debatable. Numerous data obtained on tungsten and molybdenum using a flash traditionally are interpreted as an evidence of the molecular nature of the β-CO chemisorption (exceptions include [24, 25], where the dissociative model is discussed). On the other hand, Gillet et al. [20] and Felter and Estrup [26] studied chemisorptions energy by electron diffraction using Auger electron spectroscopy, photoelectron spectroscopy, and energy losses. Thus the results of these studies present a strong evidence for the dissociation of the CO molecules in β-chemisorption on molybdenum and tungsten. Summarizing the results available, Guillot et al. [27] concluded that at the flash the β-phase likely goes into the dissociated state and without dissolving in the metal lattice, "flies" off from the surface as a result of the recombination desorption. Refractory metals of Groups 5 and 6 (titanium, zirconium, vanadium, niobium, tantalum), dissolving interstitial impurities well, chemisorbed CO so firmly ($Q_{CO} \geq 100$ kcal mol^{-1}) that already at room temperature, the rapid dissociation of the CO molecules is observed on the surface of these metals. The

dissociation flows substantially by inactivated adatoms and accompanied by dissolving oxygen and carbon in the volume of the metal substrate [28-32]. During a flash, long before the intense CO desorption, in the adfilm and between the adsorbed particles and the particles dissolved in the surface layer, a quasi-equilibrium is established: $C_{ads} + O_{ads} \rightleftharpoons \beta\text{-CO}; C_{ads} \rightleftharpoons C_{dis};$ $O_{ads} \rightleftharpoons O_{dis}$, against which the dissolution and diffusion of carbon and oxygen into the sample occur. The subsequent CO desorption is of a "two-phase" character: after the removal of the thermal dissociated surface phase (a fast step) the CO removal is observed as a result of diffusion of solute atoms of carbon and oxygen on the surface, which appears in the spectra of the thermal desorption as slowly decaying "diffusion tails" [31].
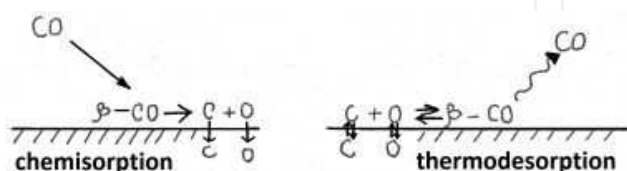

Thus, the results of studying the interaction of CO with transition metals indicate that the reaction $C_{ads} + O_{ads} \rightarrow CO_{ads}$ on the surface of platinum, palladium, rhodium, nickel, iron, cobalt, and rhenium proceeds virtually irreversible ($k_d \gg k_D$). Therefore, the controlling step is the release of CO from the dissociated phase ($C_{ads} + O_{ads}$). On the surface of such refractory metals as vanadium, niobium, tantalum, titanium, and zirconium, the quasi-equilibrium $C_{ads} + O_{ads} \rightleftharpoons CO_{ads}$ has been set in the adfilm against which the CO release in the gas phase is controlled by the desorption rate from the molecular state $CO_{ads} \rightarrow CO_{gas}$ ($k_d \ll k_D$). Apparently likewise the CO release proceeds from the surface of molybdenum and tungsten, although currently this view is not universally accepted.

2.7. Refining refractory metals from carbon and oxygen

A question on the reasons why some metals in the liquid and solid state cannot reach the thermodynamically predicted traces of carbon and oxygen during vacuum processing is repeatedly discussed in the literature. The studies of the interaction of liquid iron, niobium, and molybdenum with gaseous CO are performed, and attempts were made to eliminate the main drawback inherent in earlier works – the contact of the melt with the material of the crucible. Unfortunately, all of the experiments and their interpretations are clearly insufficient for an unambiguous and consistent description of the processes occurring in these complex systems, and have another drawback: a holistic approach to metals of the "iron triad" and to the refractory metals of Groups 5 and 6. All these metals are fundamentally different objects in terms of the removal mechanisms of carbon and oxygen. Iron, cobalt, and nickel have a single, common for carbon and oxygen "channel" in the form of the CO (CO_2) desorption. From refractory metals, oxygen can be desorbed together with carbon and in the atomic state, as well in the form of oxides. Thus, if the appearance of the "limit" contents during degassing of iron and its analogues is difficult to explain within traditional concepts of the reaction, at the degassing of refractory metals, carbon content should be limited is an obvious necessity. On the other hand, since carbon "alone" substantially cannot be desorbed from refractory metals

at high temperatures, the carbon release during vacuum processing occurs only as a result of its reaction with oxygen diffusing to the metal surface.
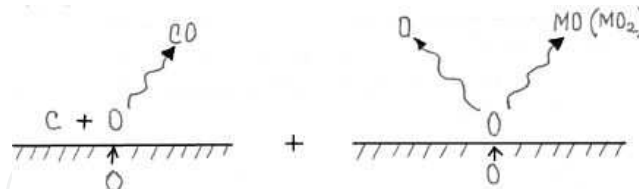
The question of what are the patterns of this interaction, which is one of the central problems of obtaining high-purity refractory metals, is repeatedly discussed. However, in contrast to the above two-component solutions of metals with hydrogen, oxygen, or nitrogen, the consistent theoretical analysis of the kinetic behavior of carbon and oxygen in the thermal desorption from solutions M-O-C hitherto substantially is not performed. Because of this, a reliable basis for making and interpreting relevant experiments is missing, and the main reference for the forecasting decarbonization capabilities of refractory metals in vacuum is the study of a thermodynamic equilibrium of the reaction $C + O \rightleftharpoons CO_{gas}$. Table 7 summarizes the equilibrium constants of this reaction on thin films of tantalum and niobium and on levitated liquid droplets of niobium and molybdenum [33–37]. These data show that the equilibrium pressure P_{CO} over solutions of (C+O) in tantalum, niobium, and, especially, molybdenum is very high (Figure 2). Thus, it is supposed [34, 37–41] that when an excess of oxygen (compared to carbon) is added to the solution, the vacuum processing of those metals should be finished with very low contents of carbon and oxygen.
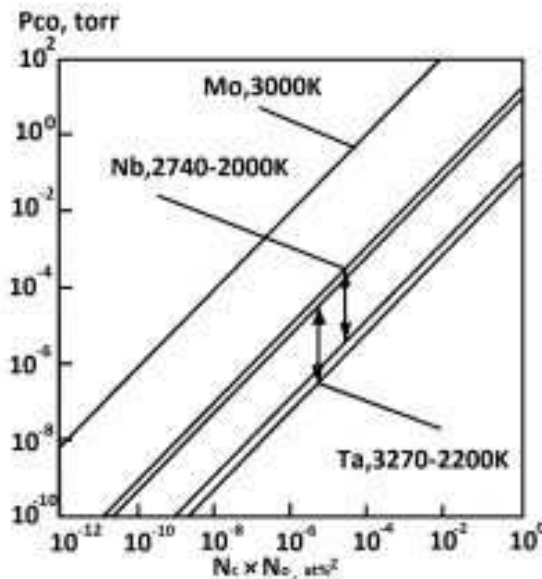

Figure 2. The equilibrium pressure of CO above the carbon and oxygen solutions in niobium, tantalum and molybdenum

According to Figure 2, at a pressure of 10^{-8} Torr the equilibrium contents of the CxO product in the solution for niobium varies from ~7 × 10 (at.%)^2 at 2000 K to ~9 × 10 (at.%)^2 at $T \approx T_m$ and for molybdenum, the value is ~(10–12) × 10 (at.%)^2 (at.%)^2 at 3000 K. Meanwhile, attempts to establish a certain correlation between the ratio O/C of the concentrations of carbon and oxygen in initial samples, and a minimum concentration of carbon, which can be achieved under UHV annealing or melting niobium, vanadium, and molybdenum, have shown that even the sample contains the considerable supersaturation with oxygen (O/C ≥ 10), the carbon content in the volume cannot be reduced more than 10–10^2 times, and to less than 10^{-2}–10^{-3} at.%. In those cases where the initial carbon content is ~10 at.% and lower, the introduction of oxygen into the solution up to 0.5 at.% does not lead to any appreciable reduction of the carbon content in general, although P_{CO}, corresponding to the current product of the carbon and oxygen contents in the solution, is higher on several orders of magnitude than the actual vacuum in the vacuum chamber. To explain these results, the suggestion is made that after achieving certain "super-equilibrium" product of contents (CxO)$_{crit}$, the surface reaction $C_{ads} + O_{ads} \rightleftharpoons CO_{gas}$ is slowing down sharply [36].

System	Constant of reaction, K_p, (at.%)^2/torr	Temperature, K
Nb-C-O	6.4 × 10^{-7}exp(67 kcal (RT)$^{-1}$	1,900–2,200
	0.21	1,850
Ta-C-O	8.3 × 10^{-6}exp(65 kcal (RT)$^{-1}$	2,000–2,300
Mo-C-O	1.5 × 10^{-4}	3,000

Table 7. Equilibrium constants of reaction $C + O \rightleftharpoons CO$ for some refractory metals

The concepts are developed according to which such situation would occur when the characteristic time between acts of the recombination of adatoms of carbon and oxygen becomes equal to the characteristic lifetime of some hypothetical active sites necessary for the exchange of the excess energy of the excited CO molecules [38-41]. Without dwelling on the detailed critique of such ideas, we merely point out that they are clearly contrary to well-established provisions of the chemical kinetics, and attempts to analyze them on the basis of the facts have an openly fitting character. Some researchers have a different point of view and linked the "discovery" of a sharp slowdown of the interaction of carbon and oxygen at low concentrations of carbon to an insufficient sensitivity of conventional methods of analysis, located at the level of 10^{-2}–10^{-3} at.% of carbon. They convincingly demonstrate this by applying the activation method by ^{3}He ions for the registration of residual concentrations of carbon with a sensitivity of 10^{-6} at.%. Indirectly, the same data show a high ratio of the electrical resistivities at room and liquid helium temperatures, which could be obtained as a result of high vacuum annealing pre-oxidized foils or thin wires of niobium and tantalum. Kulikov [19], emphasized the influence of the kinetic factors on the decarbonization processes, and the lack of reliable experimental data on the interaction of carbon and oxygen in metals of Groups 5 and 6 are associated primarily with an insufficient regard of the following two factors: the specific

surface of the molten metal and the diffusion inhibition in its volume. The reduced specific surface of the melt leads to a proportional decrease in a rate of the refining and an increase in duration of the removal of oxygen and carbon. An increase in the diffusion paths affects the reduction of the diffusion flow of impurities to the surface desorption in a quadratic dependence. Describing the issue of the laws of interaction of carbon and oxygen in refractory metals in general, we can state the following:

a. The only reliable data that would reveal the intensity of the interaction of dissolved interstitials in refractory metals are obtained from the study of the thermodynamic equilibrium of the reaction $C_{dis} + O_{dis} \rightarrow CO_{gas}$ (the temperature dependence of the equilibrium constant, the heat of dissolution of CO in metals).

b. Except for a few attempts to empirically establish the correlation between the ratio of the initial contents of oxygen and carbon, and the residual carbon content in the solution, the interpretation of results is based primarily on an intuitive basis and is largely controversial work. The systematic experimental study of the kinetics of the interaction of carbon and oxygen in vacuum processing, which should be carried out, is almost absent. A clear picture of the overall behavior of oxygen and carbon is not substantially present.

This is due, on the one hand, to the lack of a consistent theoretical analysis of patterns of the thermal desorption of both interacting impurities of different kinds, that is, with the lack of a sound basis for setting and interpretation of the relevant experiments, and on the other hand, from a purely methodological difficulties of simultaneous recording of kinetic changes of the carbon and oxygen concentrations in the process of annealing or melting. Studies on obtaining pure refractory metals in vacuum by electron beam melting (EBM) and by electron-beam floating zone melting (EBFZM) have been done for a long time. Since EBM and EBFZM have some significant differences (EBM – the presence of the mold, the drip process; EBFZM – the float-zone melting, a convective mixing of the liquid zone), it seems reasonable to consider some results of the studies using these techniques separately.

2.8. Refining refractory metals by EBFZM

If the removal of nitrogen and hydrogen (and in some cases, of oxygen) from refractory metals is the ample high-vacuum treatment of solid or molten samples, for the removal of carbon the rationality of using this treatment remains problematic. Difficulties are encountered in obtaining the "carbon-free" refractory metals of Groups 5 and 6, and a lack of clear understanding of the nature of the processes occurring in their decarburization lead to the fact that the problem of the removal of carbon (as, indeed, and oxygen) is seen as "the cornerstone" of metallurgy of pure refractory metals. Although the issue of the removal of oxygen from these metals is more or less clear, however, the existing experimental data suggest rather an inability to remove oxygen from the metals of Groups 5 and 6 by the evaporative deoxidization or the deoxidization by carbon. Apparently, there is a need to emphasize once again a very important aspect of the problem. Data on the kinetics and thermodynamics of these processes do not have an experimental evidence due to the limited opportunities of the existing melting methods and the absence of clear theoretical concepts, but also because of the low sensitivity of the analytical

methods used. Essentially, none of the known conventional physical-chemical analysis methods (vacuum extraction, mass-spectrometry, the coulometric method, and so on) do not allow for a reliable analysis of carbon and oxygen at concentrations below ~10^{-3}%. Using the method for determining the relative residual resistance (RRR) only allows to characterize the purity of the metal integrally, but in any case do not provide insight into the behavior of the impurities content. Perhaps only the emergence of new nuclear-physical methods of analysis with the removal of the contaminated surface layer would clarify the details of the behavior of individual impurities in low concentrations.

Niobium. Experimental studies aimed at obtaining high-purity niobium showed a steady growth of RRR, while reducing the amount of interstitial impurities [42–44] and the volatility of metal impurities (tantalum, tungsten) [45]. In early stages of research for refining processes of niobium there were used only EBFZM and EBM methods. The contribution of various metallic and nonmetallic elements in the value of RRR is studied: it is shown that the most significant is the effect of interstitial impurities (Fig. 3):
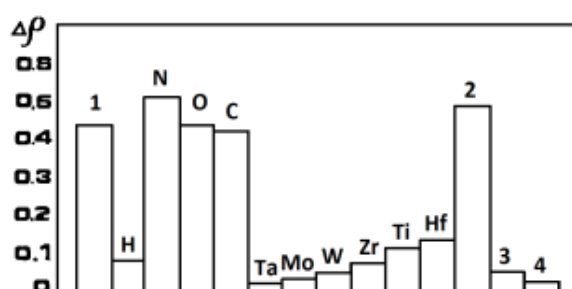

Figure 3. Influence of metal impurities and gas interstitials on RRR [42].

It is found that the effect of the zone processing by EBFZM of niobium plays a minor role (as, indeed, in the case of other refractory metals) [43]. During EBFZM, the molten metal zone is protected from the interaction with the components of the gas phase in the "cloud", formed of niobium vapors. While in accordance with the thermodynamic and kinetic data it is more advantageous for impurities to be removed from the liquid phase than from the solid; however, the lowest concentration of interstitial impurities are obtained by degassing niobium samples in the solid state. Furthermore, during vacuum melting zone the continuous interaction between solid portions of the heated sample with residual gases can occur, i.e., it is possible that interstitials would dissolve again in the metal at $T<T_m$. Many researchers used the high-temperature UHV treatment [42–45]; however, it turned out that it is impossible to obtain a high-purity niobium, even with such processing, without using other purification methods of niobium in parallel. As a result of the detailed analysis of the available experimental data, we propose the following scheme for the production of high niobium: the chemical purifying niobium powders, compacting of niobium powders, EBM of the PM rods in a high vacuum, electrolytic refining of vacuum-melted rods, EBFZM of the compacted feeds under high vacuum, and UHV annealing the cast rods (single crystals). However, even with such a

complex scheme, the "carbon-free" high-purity niobium could be obtained with a great difficulty, so that there is still no clear idea on the effective decarburization process of niobium. It is quite possible that by variation of the ratio C/O in the initial specimens of niobium and by variation of the partial pressure P_{CO} in the gas phase, the niobium specimens with a low content of both interstitials could be obtained. A number of studies determine the relationship between the equilibrium concentrations of oxygen in niobium and the oxygen partial pressure P_{O2} in the vacuum chamber. Even an attempt is made to evaluate the influence of the gas phase in a vacuum chamber at the carburization or decarburization of solid niobium specimens.

Molybdenum. The available experimental information on the influence of parameters of EBFZM such as the number of zone passes, the rate of recrystallization, the purity of feeds, vacuum, etc., on the behavior of non-metallic and metallic impurities in molybdenum is clearly insufficient. It is found that the predominant process of EBFZM of molybdenum is the evaporation of impurities while a minor effect is of the zone effect, confirming by the micro-hardness or RRR on the length of single crystals of molybdenum. Noted that after the multi EBFZM of molybdenum the single crystals have the high degree of purity: RRR values reach 15,000–30,000. However, there is a noticeable unevenness in the distribution of impurities along the length and radius of crystals: the single crystal of molybdenum of 120 mm long after eight zone passes at a rate of 5 mm/min has a value of RRR varied from 17,000 to 1,000. It is unlikely that this change of RRR occurs only due to the zone effect. Increasing the number of zone passes, and thus the exposure of molybdenum in the liquid state in a vacuum, results in an increased purity. However, results of many studies diverge markedly in the quantification of this effect. Greater certainty exists regarding the degree of vacuum: the purity of molybdenum significantly enhanced by the use of the oil-free vacuum and UHV.

Tungsten. The effect of interstitials on physical and mechanical properties of tungsten is significant. Therefore, repeated attempts to get a clearer picture of the behavior of these impurities (in particular, carbon and oxygen) during EBFZM are done. Usually, the first zone passage is the most effective in the purification of tungsten: the RRR value is at 21,000–25,000, and the oxygen content decreases from 2×10^{-3} to 3×10^{-4}%. Thus, the carbon content is reduced from 2.5×10^{-3} to $(4$–$20) \times 10^{-4}$%. Several studies have noted that multiple zone passes do not result in the complete removal of oxygen and carbon from tungsten (it seems this process is endless). However, these findings cannot be considered conclusive because the impurities are often found at the detection limit of the analytical methods (even of the most sensitive), and therefore could not give reliable information about the behavior of these impurities. It is shown that, depending on the quality of the vacuum and the growth rate of tungsten single crystals, the RRR values range from 13,600 to 99,300. An application of the activation by ^{3}He ions, allowing defining the content of carbon and oxygen to $\sim 10^{-7}$%, allow establishing a definite link of melting conditions with a final content of these impurities in tungsten. It turned out that the content of oxygen and carbon in the tungsten specimens does not exceed 1×10^{-4} at.%. The study of behavior of the same impurities by the same method in tungsten alloyed with rhenium shows that the carbon content in the tungsten after a zone refining does not dependent on the content of rhenium and is at 1×10^{-5}%, while the oxygen content is strongly dependent on the content of rhenium and is at a minimal level ($\sim 5 \times 10^{-6}$ at.%) at 2–5% rhenium. At these

contents of rhenium, the oxygen content is for about an order of magnitude lower than in pure tungsten melted under similar conditions. Some authors believe that there is an additional deoxidation by rhenium and this process is very similar to the deoxidized metals of the "iron triad" group by some element-reductants [19]. It should be noted that the majority of the studies using EBFZM is aimed mainly at obtaining and characterization of single-crystal samples, rather than on finding and understanding of a consistent behavior of interstitial impurities. Therefore, data on the behavior of interstitial impurities are few and uninformative, as the analytical methods used do not exclude the influence of the surface oxides and other contaminations of samples, which is very significant in the determination of small amounts of impurities, and therefore do not give a true picture. Therefore, it is necessary to conduct a correct and consistent study of the behavior of impurities (especially interstitial impurities oxygen and carbon) in metals such as niobium, molybdenum, and tungsten. Particular attention is paid to the systematic application of more sophisticated and sensitive analytical methods to remove surface contaminations from samples prior to analysis.

2.9. Theoretical model of the removal of interstitials from refractory metals

The results of our theoretical investigation of the interaction of carbon and oxygen in the solid and liquid refractory metals in vacuum are presented here briefly. Although the results are general in the nature, the presentation is mainly applicable to metals of Group 5 and 6 of the Periodic Table that are the most extensively studied in aspects of the interest to us. The basic model is given by sequence of the segregation of carbon and oxygen atoms from the volume of metals in a vacuum, as shown schematically in Figure 4 [46–53]. Earlier, during the discussion of the fundamental issues associated with the interaction of impurities a similar conceptual approach has been developed, using the similar notation, terms, and equations. This greatly simplifies the description and understanding of our theoretical model together with the fundamental issues made before us.
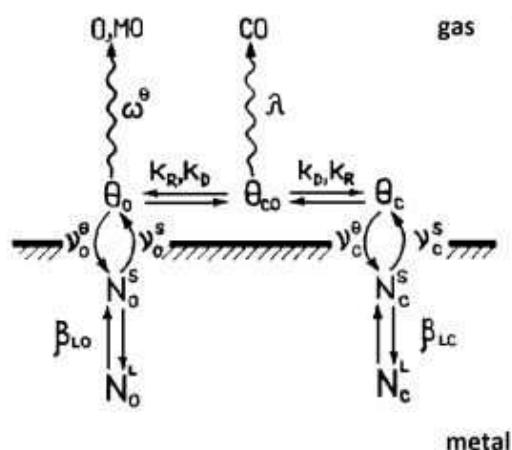

Figure 4. Model of the carbon and oxygen removal.

Carbon atoms diffuse into the subsurface layer and then bypass the phase boundary and on the surface recombine with the oxygen adatoms with the formation and subsequent desorption of the CO molecules. For oxygen adatoms impinging on the surface in a similar manner, there are two possibilities: either recombine with carbon adatoms and desorb as CO or forming a chemical bond with the metal atoms, and desorb as monoxide MO (at high concentrations of oxygen, in the form of MO_2). In formulating a system of nonlinear boundary value problems of diffusion, which allows to describe the kinetics of these processes, it is assumed that the metal that isothermally annealed in vacuum at a temperature T has the form of an elongated plate, of an extended half-thickness cylinder or a sphere of a radius R, and in the volume of metal in the initial moment of time the carbon and oxygen atoms with the contents of $N_c(0)$ and $N_o(0)$ are uniformly distributed. Boundary conditions for the corresponding one-dimensional diffusion equations are found by matching the flux densities of diffusion $J^D|_s$, segregation $J^{s\theta}$, and desorption J^d of each impurity on the metal surface (the principle of the quasi-equilibrium)

$$J_i^D\big|_s = -\left(D_i / v_s\right)\left(\nabla N_i\right)\big|_s = J_i^{s\theta} = J_i^d$$

are written with an assumption that (a) the adfilm is sparse, (b) the lateral interactions in the adfilm can be neglected and (c) the contents of both impurities in the solution are much lower than the solubility limit. The comparison of the flux densities of the carbon desorption $J_c^d = \Gamma^\theta \theta_c \theta_o$ and of the oxygen desorption $J_o^d = J_c^d + \omega^\theta \theta_c$ (where Γ^θ is the constant of the rate of the CO molecules desorption from the atomic phase $O_{ads} + C_{ads}$, ω^θ the constant of the rate of the monoxide MO desorption (for metals of Group 6, atomic oxygen), θ_i the degree of the surface coverage of the metal adatoms of grade i) shows that there is some critical degree of the surface coverage by carbon $\theta^* = \omega^\theta / \Gamma^\theta$, when the desorption of oxygen has been changed dramatically: in the overcritical region $\theta_c/\theta^* \gg 1$ oxygen desorbs mainly together with carbon, while in the subcritical region $\theta_c/\theta^* \ll 1$ oxygen desorbs predominantly "by itself" (as MO or O) and almost does not "feel" the presence of carbon in the metal. Thus, the value of θ^* sets the characteristic scale the covering of the surface, and the corresponding critical content of carbon $N^* = \omega/\Gamma$ is the characteristic scale of contents in the solution. Here, $\omega = \omega^\theta f_o$ and $\Gamma = \Gamma^\theta f_o f_c$ the effective constants of the desorption rate from the subsurface layer of metal in a vacuum, respectively molecules of MO (O) and CO, f_i the coefficient of surface segregation. With this type the oxygen content $\xi = N_o/N^*$ and the carbon content $\eta = N_c/N^*$ are introduced. Based on the assumption of the quasi-equilibrium of the surface segregation of oxygen and carbon, and after appropriate dimensionless procedures the boundary conditions are obtained, which have defined a system of nonlinear boundary value problems of diffusion of carbon and oxygen. Further study of this system is carried out in the following sequence: first, the subcritical region of the carbon contents is considered and focuses on the behavior of the average volume contents of carbon and oxygen, and the connection between them, the results are then summed for the whole content region of carbon and, finally, the disclosed features of behavior patterns of the surface content of carbon in the high temperature annealing in vacuum. A particular

attention is given to the limit degree of the refractory metal decarburization $L = \eta(0)/\eta_\infty$, which can be achieved under specified conditions of the high vacuum processing (impurity composition, geometry and size of the sample, temperature, vacuum). It turned out that, contrary to traditional notions the decarburization degree L is determined by the oxygen supersaturation of the metal not on the initial carbon level, but on the characteristic for each metal a critical value $N^*(T)$. There is a strong dependence of the decarburization degree L from the effective size of the sample. Upon annealing of thin samples, the decarburization degree L is maximal and depends on $\xi(0)$ exponentially strongly and large even at the low oxygen saturations over the critical value N^*. Upon annealing of bulk samples, L is minimal and depends on $\xi(0)$ weakly root-like and is small even at the significant oxygen saturations over $N^*(T)$. The temperature dependence of the decarburization degree L is determined mainly by the temperature dependences of the critical concentration of $N^*(T)$ and the characteristic size of the sample $R^*(T)$. With decreasing the annealing temperature the value of N^* decreases sharply, and R^* increases dramatically: the first is equivalent to the "temperature" introduction of oxygen into the sample, and the second the "temperature" reduction of its effective size. As a result of the joint action of both factors, the decrease of the annealing temperature (within certain limits) should lead to a significant increase in the decarburization degree of the metal. An exposure to the gas phase becomes noticeable from the certain critical density of the adsorption flow α^*. If $\alpha_{ads} \leq \alpha^*$, the annealing of the metal occurs in the same manner as in conditions of an absolute vacuum, that is, the carbon content always reaches its maximum level ($L^v \approx L$). In the case $\alpha_{ads} \leq \alpha^*$, it, before reaching the limit, passes through minimum ($L^v \approx L$), and then increases at a rate proportional to α_{ads}. In both cases, the high decarburization degree of L can be achieved only if $\alpha_{ads} \ll 1$, and at high flux densities $\alpha_{ads} \gg \alpha$ the dependence of L on the initial supersaturation of the sample with oxygen dramatically weakens: in the limit of thin samples instead of the strong exponential dependence it becomes linear, and in the limit of massive samples it "disappears" at all. As the annealing temperature is lowered, the value of α_{ads} rapidly increases, and of $\alpha =$ decreases rapidly, so that below the certain temperature T_m the effect of adsorption becomes dominant and the decarburization degree L of metal falls. As increasing the oxygen content in the metal, as an increase in the effective pressure of CO in the system, leads to a shift in T_m to higher values. The quantitative results (in the form of appropriate tables and graphs) obtained in these studies provide the basis for selecting the optimum conditions for the high-temperature annealing of the refractory metals. Because the patterns of the carbon and oxygen interaction in the process of the thermal desorption of the liquid refractory metals are of a considerable interest for vacuum metallurgy, the issue is given special attention. A distinctive feature of the process of allocating the impurities of carbon and oxygen in the liquid metals, as compared with the solid ones, is complicated by a transport of them to the metal surface (molecular diffusion plus convective mass transfer). The intensity of this transport depends on the direction and rate of the hydrodynamic flow in the volume of the liquid metal. The basis for describing the kinetics of the process served a model of a δ-layer. Under this model, it is believed that mainly in the core melt due to convective mixing, the impurity is distributed uniformly with a certain concentration of N_L. The diffusion "resistance" or "braking" is mainly concentrated in a narrow subsurface layer of a thickness δ. Within this layer the transfer is carried out by the molecular diffusion with the flux density

$$J_{i\ s}^{D} = -\left(v_a \propto\right)^{-1} \dot{N}_L = \frac{\beta_L}{v_a}\left(N_L - \dot{N}_s\right) \tag{23}$$

Here N_s is the surface impurity concentration, α the specific surface of the melt, $\beta_L = D/S$ the mass transfer coefficient, which is the main parameter of the model and is generally determined experimentally. In typical cases, β_L is 10^{-1}–10^{-3} cm s^{-1} and δ is 10^{-2}–10^{-4} cm. A chain of equations (23) together with the consistency conditions of the flux densities of diffusion, segregation, and desorption of carbon and oxygen leads to the corresponding system of nonlinear differential equations, which shows that the previously defined patterns of the interaction between carbon and oxygen at the high-temperature annealing of refractory metals in the solid state in this study remain valid. In the case of the liquid metal, with the difference that in the case of the melt instead of the relative diffusion mobility of the impurities, the relative coefficient of the mass transfer occur and instead of the effective size of the solid specimen, the effective thickness of the δ-layer.

2.10. Experimental verification of the model

The experimental verification of the model was carried out on the solutions of carbon and oxygen in two metals (niobium, molybdenum) by two crucibleless melting methods: the high-frequency vacuum levitation melting (HF VLM) and the electron-beam floating zone melting (EBFZM). They are shown in Figures 5 and 6. In Figure 5 the liquid droplet (red) is shown inside the water-cooled cupper electromagnetic inductor (partially seen). The lines of the high-frequency electromagnetic field, which supports the levitated droplet, are shown by dashed lines. The volume of the levitated droplet is about 2.0–3.5 cm^{-3}, depending on the nature of the metal.
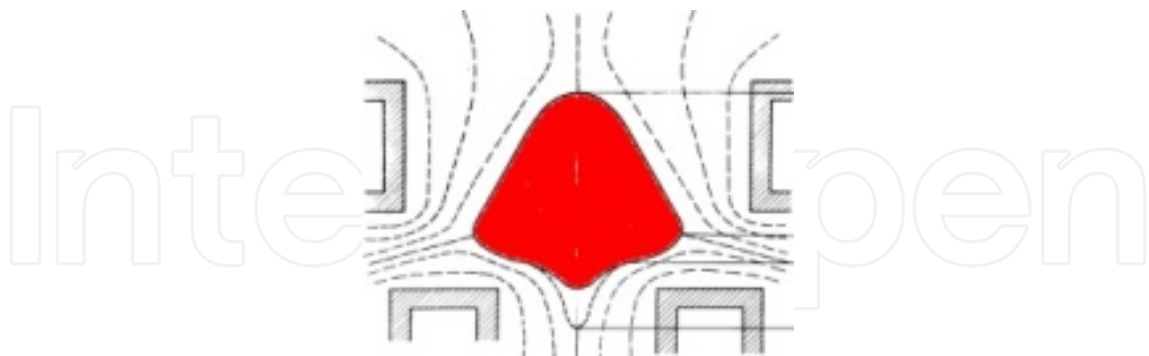

Figure 5. High-frequency vacuum levitation melting.

In Figure 6 the set-up for electron-beam floating zone melting is shown. The liquid zone is shown by red color. Here, the liquid zone does not contact with any contaminating materials like refractory crucible materials, except two interfaces with a feed and a grown crystal. The volume of the liquid zone is about ~2.0 cm^{-3} depending on the nature of the metal, dimensions of a growing single crystal, and the height of the liquid zone.
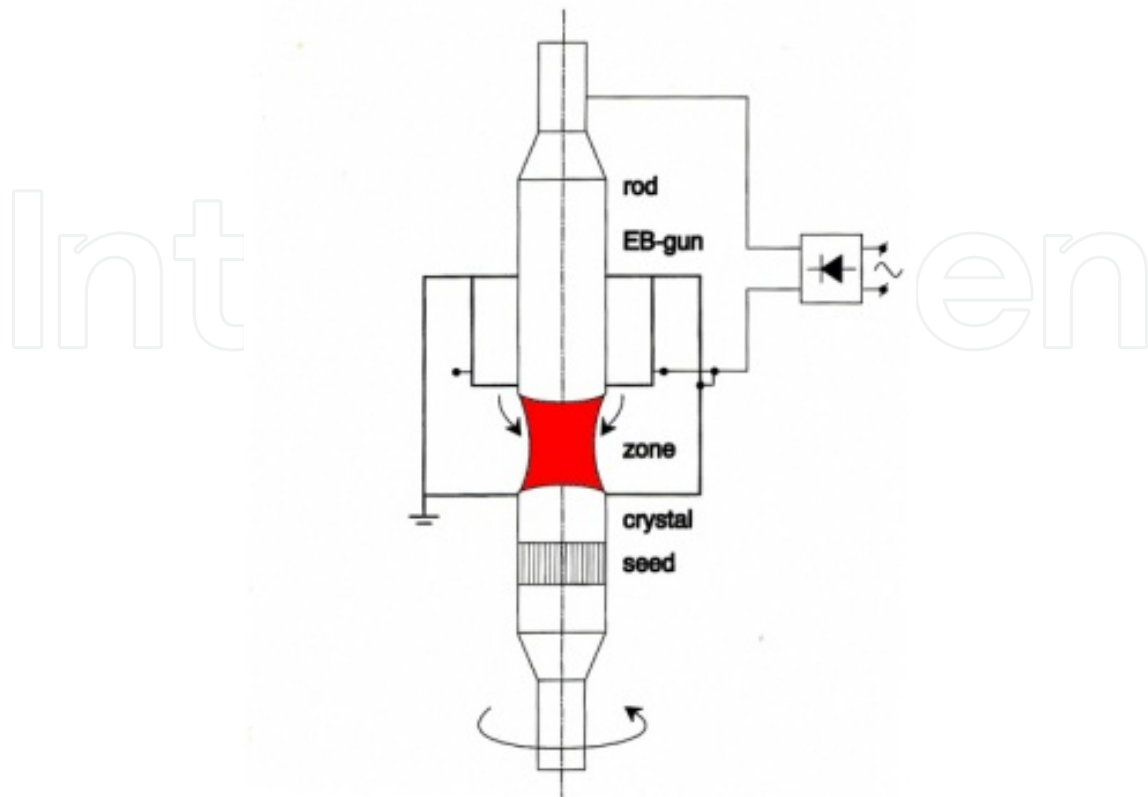
Figure 6. Electron-beam floating zone melting.

Specifically, the demonstration of validity of the basic provisions of the proposed model has been performed on niobium and molybdenum [53–55]. Both metals are excellent examples of the low solubility of carbon and oxygen, and the possibility of removing carbon by oxygen in an atomic state. In the case of niobium four series of samples with the oxygen content of 0.93 at.% and and the carbon contents of 0.35, 0.58, 0.83, and 1.05 at.% were prepared. The temperature of the levitated liquid drop of niobium is 2850 ± 50 K. The kinetics of the mean concentrations of oxygen and carbon in niobium for all four series are shown in Figure 7. It can be seen that the transition from the series 1 (O/C ≈ 9) to the series of 4 (O/C ≈ 6) leads to a sharp change in the slope of the curves in both graphs.

This, on the one hand, confirms the assumption of the high mass transfer rates in the levitated niobium drops and, on the other hand, indicates the occurrence of an experiment in a super-critical range of both impurities. In accordance with the model representations [46], an experimental verification of the model and a determination of the critical concentration N* is possible by simultaneous recording the behavior of the average concentrations of carbon and oxygen in the high-temperature vacuum treatment.

$$\partial \ln <N_c> / \partial \Delta \qquad (24)$$

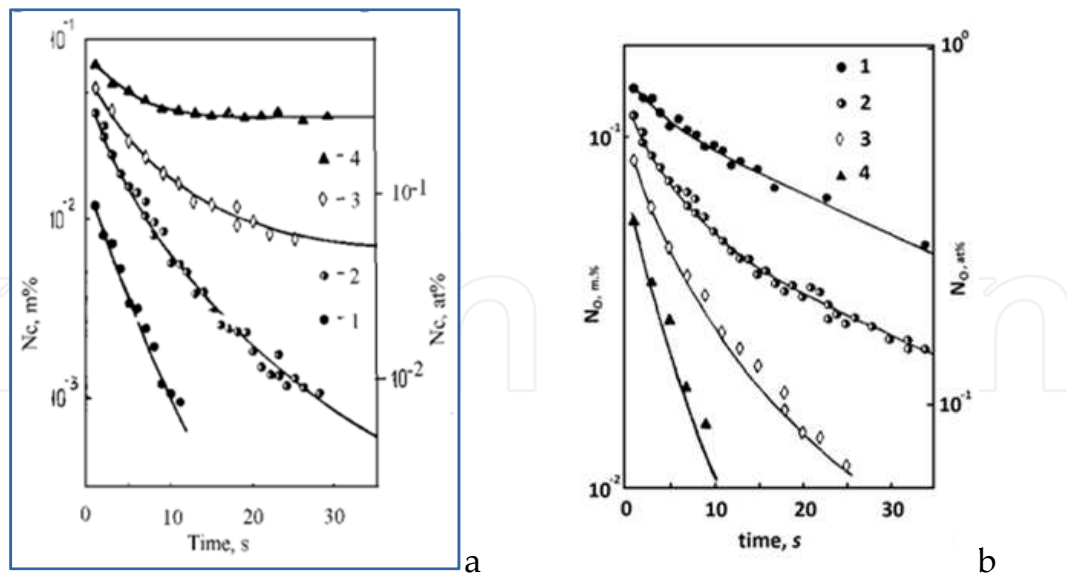**Figure 7.** Kinetics of mean concentrations of carbon (a) and oxygen (b) in niobium.

Here, $\Delta = <N_o> - <N_c> + N_c^\infty$, and S is the parameter characterizing the relative intensity of diffusion and desorption flows. From expression (24) it is understood that the dependences $<N_c(t)>$ and $\Delta(t)$, obtained by annealing of samples with different ratios of the initial contents of carbon to oxygen should "stack" on one line in the coordinates $\partial\Delta/\partial\ln<N_c> - \Delta(t)$, with a slope $1/S$ and the initial ordinate N^*. In full accordance with the predictions of the model, the dependences $\ln N_c = f(\Delta)$, constructed from the experimental data (Figure 8), are close to linear and are almost parallel. The critical content, determined from the slope of the curves, taking into account the contribution of desorption of molecules NbO_2, is equal to $N^* = 0.05 \pm 0.01$ at. % and $S > 50$. Based on the values of N^* and S it is possible to directly compare the calculated and experimental carbon and oxygen behavior in time. Since when $S > 50$ the kinetics is "insensitive" to the value of the effective thickness of δ-layer, it is assumed that $q \to 0$ as $S \to \infty$ and the corresponding system of nonlinear differential equations are numerically solved, with $N^* = 0.05$ at. % and $t_o = 43$ s (the relaxation time of the release of oxygen is found from experiments with samples of niobium doped with oxygen only). The initial conditions are used in the calculation of the content of oxygen and carbon in 1 second after melting, and then the results of numerical calculations are compared with experimental data. For all four series studied of the niobium alloy doped with both impurities there is a good agreement between theory and experiment. This is a direct experimental proof of the validity of the model in a wide range of impurity concentrations.

Experimental study of the removal of carbon and oxygen of niobium using sensitive methods of activation analysis (neutron and deuteron) are conducted in two directions: the study of the behavior of oxygen in carbon-free niobium and study of the joint behavior of carbon and oxygen in the process of multiple EBFZM. It has been established that oxygen and carbon are uniformly distributed over the entire length of the crystals except unsteady region in the initial portion of the crystal. The dependence of the full residual pressure in the melting chamber is
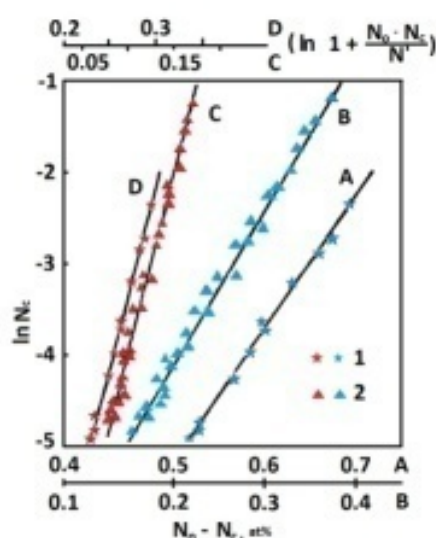
Figure 8. Dependences $\ln N_c = f(\Delta$, constructed on experimental data. In accordance with theory, they should be linear and parallel (A – B & C – D)

found from the number of passes and the warm-up mode of the melting chamber. Figure 9 shows the dependence of the oxygen content on the stationary portion of niobium single crystals of the number of zone passes for three preheat (I- 1 h, II- 3 hours, III- 5 h), obtained from the study of 23 crystals. At first, to illustrate the effect of surface contamination in the determination of small amounts of interstitials, the results of the determination of oxygen by vacuum melting, mass spectrometry, and fast-neutron activation are done without etching the surface of the sample before measuring the activity. It also shows the data obtained by NAA and ^{3}He activation with a careful removal of contaminated surface layers of a thickness of at least 10 microns (of the same samples). The data indicate a good agreement between the two methods of activation analysis with the removal of the contaminated layer. At the same time, the discrepancy between the data received by "traditional" methods (vacuum-extraction, coulonometry) with the similar removal of the surface layer and two activation methods with the removal of the oxidized layer is almost two orders of magnitude for the same samples. This is strong evidence in favor of the use of highly sensitive methods of analysis for deter-mining the oxygen concentration below 10^{-3}%. The difference in the slope of the kinetic curves for different modes of the melting chamber warm-up due to the influence of the residual atmosphere (especially moisture). The results of this work are shown that the mechanism of the oxygen removal from the liquid niobium remains constant over a wide range of oxygen concentrations from 10^{-2}% to 10^{-5}%. Data obtained earlier by other authors on changes in the mechanism are due, apparently, to the incorrect determination of the oxygen content by conventional analytical methods.

When the flow of the two competing processes (desorption of oxide layers of niobium and carbon monoxide from the surface of the molten zone) have a situation where at a certain critical oxygen content the carbon removal slows down sharply, but oxygen in the form of oxides of niobium continues to be desorbed. As a result of the multiple EBFZM of niobium
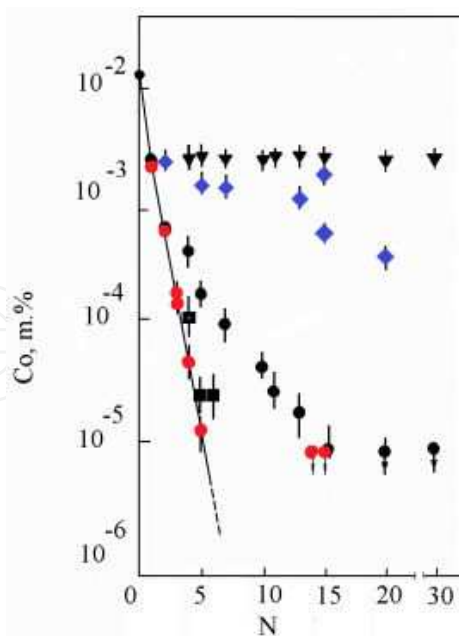
Figure 9. Dependence of the oxygen concentration on the stationary part of niobium single crystals of the number of zone runs; single samples of every run were analyzed by several analyzing techniques: ○,●– NAA (red & black, two different regimes of heating-up the chamber), ■ – ^{3}He, ▼- vacuum-extraction, samples after standard cleaning; ◊ - vacuum-extraction (blue), samples after careful cleaning (removal of a layer of at least 10 microns).

doped with carbon and oxygen, it is found that at reducing the oxygen content in the range of 6×10^{-3}% and 1.5×10^{-4}% the nature of the interaction of carbon and oxygen changes: the carbon content tends to a limiting value for the initial contents of both interstitials and the faster, the closer to the "critical" range is the oxygen content after this zone run. To reveal limits of the critical range of oxygen concentrations with greater accuracy is not yet possible because of the discrete nature of the vacuum zone melting, and the impossibility of fixing a continuous fall of the contents of both interstitials. The dependence of the degree of decarburization during vacuum zone melting from exceeding the initial oxygen concentration above the "critical" range for the crystals with the same initial value for both interstitials has been studied, and it is shown that at the transition to higher absolute contents of both interstitials, the degree of decarburization increased by more than two orders of magnitude. It is found that the decarburization efficiency of niobium depends primarily not on the ratio of the initial ratio of O/C, but on the difference between the initial and critical oxygen concentrations: the higher the difference, the more intense decarburization proceeds. The data obtained experimentally confirm the validity of the proposed model of the interaction of carbon and oxygen: when achieving the certain critical oxygen concentration, the carbon removal rate slows dramatically and establish the limiting concentration of carbon in niobium.

In similar experiments on molybdenum doped with oxygen and carbon in the wide concentration range, it is shown that during HF vacuum levitation the contents of both impurities are reduced to 5×10^{-5}% and 10^{-6}%, respectively, in approximately 15 seconds. This fact, on the one hand, also demonstrates the validity of the model proposed concerning the removal of the interstitials by forming CO and MoO_2. On the other hand, these experiments indicate that there

is no fundamental obstacle to obtaining molybdenum, substantially free of carbon and oxygen in the melt in vacuum.

3. Technological plasticity of unalloyed high-purity refractory metals produced by EBM

Practical applications of refractory metals, produced by means of EBM, are limited due to the intergranular brittleness of cast polycrystalline ingots (especially of molybdenum and tungsten), although these metals in the single-crystalline state are sufficiently plastic in a wide temperature range. It is known that interstitials are almost always present in cast refractory metals as a second phase and contribute to the appearance of cracks at grain boundaries. The low technological plasticity and structural strength of refractory metals are particularly bad at medium and low temperatures. Studies [56–58] are shown that molybdenum of vacuum melting can be of the appreciable technological plasticity if the interstitials contents are lower than $1 \times 10^{-4}\%$ of each element. These data for many years were a kind of a truth for researchers who worked on this problem. The real prospect to get molybdenum with the low content of interstitials arose with an advent of industrial vacuum electron-beam melting (EBM). However, ingots of unalloyed molybdenum of EBM, despite the relatively low content of interstitials, have still the low technological plasticity because of the increased segregation of interstitials in clusters at grain boundaries, which exceeds the average concentration of interstitials in the volume of ingots for several orders of magnitude. Since it is impossible to achieve the greater technological plasticity by vacuum melting only, the researchers direct their efforts towards the creation of alloys in which the fracturing effect of interstitials has been decreased by doping. Additives added during melting prevent the segregation of interstitials along the boundaries and bind residual interstitials in the dispersed second phase. Well-known dopants are metals of Groups 4, 5, 8, such as boron, aluminum, carbon, and rare earth metals. Currently, there is a wide range of cast molybdenum and tungsten alloys of the satisfactory technological plasticity. However, in recent decades there is a sharp increase in the interest of undoped high-purity refractory metals. This is due to the fast development of industrial areas of the critical application. Doped alloys are almost completely excluded from the practice of the thin-film metallization in microelectronics. Thus, the purity and technological plasticity of the EB-melted undoped polycrystalline molybdenum and tungsten attract attention.

3.1. Molybdenum

The low plasticity (or the high intergranular brittleness) of coarse-grained, electron-beam melted molybdenum is a well-known feature. It is believed that the brittleness may be caused by the segregation of interstitials (oxygen, carbon) at grain boundaries. A common way to avoid the embrittlement of this material consists of the addition of deoxidants or modifiers such as carbon, boron, and other elements to the feedstock before or during electron-beam melting (EBM) to produce the fine-grained macrostructure [59–62]. We have studied the possibility of improving the plasticity of molybdenum by subjecting it to high-temperature

processing. Three ways are tested for preparing pure molybdenum ingots. The first way consists of the single EBM run at the melting rate, at which ingots have the smallest grain size or the fine-grain structure. The second way is the multiple EBM run, and the third way is the duplex process consisting of electron-beam melting and vacuum arc melting (VAM). Molybdenum ingots, 80 mm in diameter and 1300 mm in length, are melted in an electron-beam furnace in a vacuum of 1×10^{-3} Pa with melting rates ranging from 0.2 to 2 kg min^{-1} [60-63]. The number of runs ranges from one to five with the melting rate ensuring the maintenance of the melt in the mould (crystallizer) at the appropriate temperature. The mean power of the EBM is 100 kW at an accelerating voltage of up to 25 kV and an emission current of 4 A. The melting of molybdenum ingots of 140 mm in diameter and 350 mm in length is performed in the VAM set-up in a vacuum of ~10^{-2} Pa at a mean voltage of 35÷40 V and an arc current of 4.5÷5 kA. Cylindrical specimens are cut out of each ingot for chemical analysis, metallography, and mechanical testing. For microfractography, flat specimens (10 mm × 10 mm × 50 mm) are cut out normal to the ingot axis. The fracture plane of the specimens is parallel to the ingot axis. The mechanical testing of the specimens is carried out by a conventional technique in an Instron machine. Light and electron scanning microscopes are used for microfractography and metallography. The grain size is determined by directed secants on the transverse and longitudinal macrosections of polycrystalline ingots. The texture of ingots is studied by observing X-ray diffraction patterns. The behavior of the material under processing conditions (pressing and forging of ingots, rolling of billets) is tested in a standard way at 900–1300°C, with the ingots heated in induction furnaces in vacuum or in a hydrogen atmosphere. Attempts to vary the melting rate over a wide range during the run in the EBM set-up of the PM feedstock are unsuccessful because the melting rate is less than 0.5÷0.6 kg min^{-1} and is limited by intensive outgassing of the feedstock and liquid metal. The EBM ingots of the first run have a coarse structure and many metallurgical macrodefects: gas voids, unmelted PM fragments, and severe fissures (Figure 10).
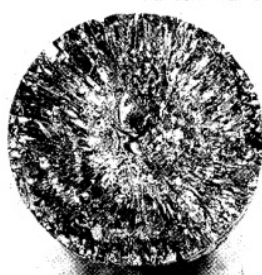

Figure 10. Gas void at the fracture surface of the molybdenum ingot (In the vicinity of a PM fragment, the center).

As usual, to produce the ingot of good metallurgical quality the second EBM run is performed at a higher melting rate. The melting rate has a strong effect on the macrostructure: the mean grain size is 5–6 mm for the low melting rate and 1–2 mm for the high rate and the grain lengths are respectively 100 mm and 10 mm or less (Figure 11).

The texture analysis shows that the grains in all ingots have a longitudinal axis close to the (001) orientation. With successive runs carried out at the rate of ~1 kg min^{-1} the average size of
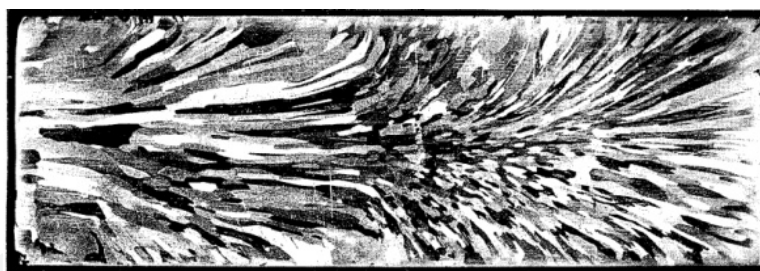
Figure 11. Macrostructure of the molybdenum ingot of 1m length after the EBM run at 0.2 kg min^{-1} (left part) and 2.0 kg min^{-1} (right part).

grains increases slightly: it is 2.2 mm after the second run and 2.7 mm after the fifth. Figure 12 depicts the grain size distribution for two macrostructures of the molybdenum ingot after two runs carried out at the rates of 0.2 kg min^{-1} and 2 kg min^{-1}.
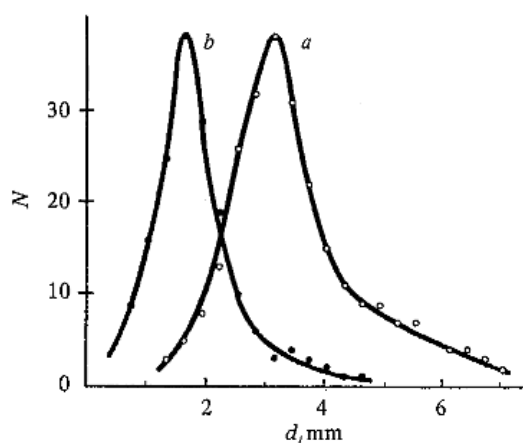

Figure 12. Grain size distribution in the molybdenum ingot after the second run by EBM at the rate (a) 0.2 kg min^{-1} and (b) 2.0 kg min^{-1}.

The etch pit density in pure molybdenum ingots decreased as the number of melts increased from one to five. The grain boundaries were less strongly etched and became thinner with increasing number of runs. As seen from Table 8, after the first and second runs all metallic impurities were near the detection limit (0.01÷0.1 ppm) of the ICP mass-spectroscopy. The tungsten content was nearly constant (~10 ppm) in the course of the runs. After the fifth run all metallic impurities and interstitials in molybdenum were below the detection limit of analytical techniques used.

In our version of the duplex EBM-VAM technique, the EBM ingots are used as an initial material and have been melted in the vacuum arc furnace with a melting rate of 2.1–2.3 kg min^{-1}. The main feature of the VAM technique is that the liquid metal is stirred by the electro-magnetic field of a solenoid mounted outside of the water-cooled crystallizer. Figure 13 depicts the grain size distribution in two molybdenum ingots produced with different stirring currents. It is seen that the macrostructure strongly depends on the stirring current. At low
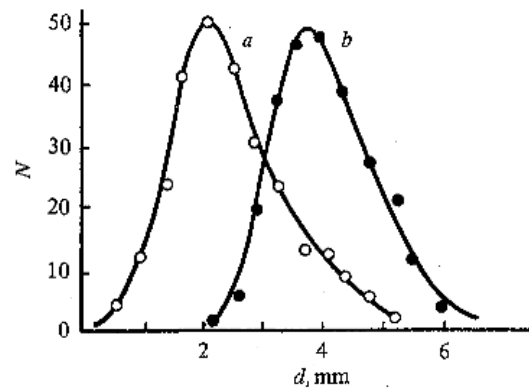
Figure 13. Grain size distribution in the molybdenum ingots prepared by duplex melting with different stirring current: (a) 1 A, (b) 4.5 A.

Number of runs	Impurity content, $10^{-4}\%$ m.							
	C	O	N	Ni	Fe	Ti	Ta	W
PM feedstock	30	40	10	2	100	5	1	20
Single run	8	2	1	<0.3	1	<0.3	1	10
Double run	8	0.5	<1	<0.3	<1	<0.3	<1	30
Fivefold run	8	<0.5	<1	<0.3	<1	<0.3	<1	30

Table 8. Impurity content in EB-melted molybdenum depending on the number of runs

stirring current (1–1.5 A) the macrostructure is characterized by grains up to 60 mm long with a mean size of 4 mm, inclined to the ingot axis by 15°. At higher stirring currents (up to 5 A) the grains are smaller (~2 mm) and shorter (~15–20 mm). The carbon and oxygen contents in molybdenum produced by the duplex melting are shown in Table 9: the higher the stirring intensity, the purer the metal. In any case, the cast molybdenum is not contaminated during arc-melting at a lower vacuum.

The normal cross-section of the molybdenum ingot of 80 mm in diameter, produced by the duplex EBM+VAM, is shown in Figure 14. Here, it can be seen the homogeneous structure with small grains, except the subsurface layer. Microfractography showed that the specimens from all ingots (EBM, EBM + VAM) have a mixed transcrystalline/intercrystalline fracture with micro-voids and inclusions on the fracture surface (Figure 15a). The relief of the fracture surface varies in the vicinity of the inclusions, indicating their influence on the plastic flow. Cracks originate near the voids or flat precipitates; Figure 15b depicts a void presumably formed as a result of the breakaway of a carbide particle.

The high-temperature plastic deformation of molybdenum ingots subjected to multiple EBM or duplex melting (except for ingots after the first EBM of the PM feedstock) occur without failure of the specimens. About 20% of the ingots tested after the first EBM run fail because of cracks during manufacturing.
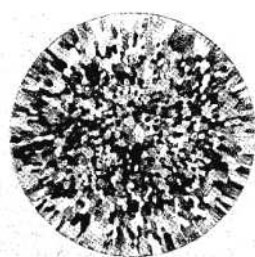
Figure 14. Macrostructure of the molybdenum ingot produced by duplex melting with the highest stirring current.

Figure 15. Fracture surfaces of molybdenum: (a) mixed fracture (double EBM run); (b) void, formed after breakaway of carbide (EBM+VAM).

The plastic deformation of 75–82% and the temperature of 1200–1300°C are chosen to produce billets with uniform grains. Sheets of 0.3 mm thickness are prepared by hot rolling. Mechanical tests show that molybdenum ingots are ductile at all stages of the high-temperature fabrication. The mechanical properties of annealed and unannealed rolled molybdenum specimens are presented in Table 9. The temperature dependence of the mechanical properties of 0.3 mm thick annealed sheets is shown in Figure 16 over the temperature interval 200°C to –192°C. The mechanical testing reveals good ductility and high strength of coarse polycrystalline ingots of molybdenum melted in the electron-beam or vacuum arc set-ups. Although information on the behavior of carbon and oxygen during vacuum melting of molybdenum is rather scant, it is known that oxygen can be removed as oxygen atoms, carbon oxides, and molybdenum oxides, but carbon can be removed only as carbon oxides. At low carbon and oxygen contents the interstitials in molybdenum behave independently: the carbon content remains constant in the course of repeated EBM, whereas oxygen content sharply decreases. Thus the vacuum deoxidation of molybdenum (or self-deoxidation), in which the oxygen removal occurs owing to the evaporation of carbon oxides and volatile molybdenum oxides can be used for the production of molybdenum ingots of high purity and good mechanical properties.

The study of ingots produced by the double EBM run reveal the significant effect of the melting rate on the macrostructure of the undoped high-purity molybdenum. The average grain size reduces from 6 to 2 mm (about 3 times) with an increase in the melting rate of 0.2–2 kg/min (i.e., 10 times). The average grain length decreases respectively from 100 to 10 mm. The ingots produced at the melting rate of 0.2 kg/min contain columnar grains, which are inclined from

the axis of the ingot. The texture analysis reveals that all ingots contained grains with the longitudinal axis close to the [001] direction.

Stirring current, A	Oxygen content, 1×10^{-4} m%		Carbon content, 1×10^{-4} m%	
	EBM	EBM-VAM	EBM	EBM-VAM
1	2	9	8	8
3	5	6	8	8
5	4	4	8	8

Table 9. Oxygen and carbon contents after EBM and EBM+VAM

Annealing temperature, ^{0}C, 30 min	σ_b, MPa	δ, %
Unannealed	990	7.5
800	835	13
900	740	22
1000	630	27
1100	640	29

Table 10. Ultimate tensile strength, σ_b, and elongation, δ, of molybdenum purified by the duplex process EBM+VAM

Increasing the number of EBM runs from 2 to 5 at the rate of melting of 1–1.2 kg/min results in an increase of the average grain size up to 2.7 mm (after five runs) at a constant length of 10–20 mm. Further reduction of impurities is able to establish only by indirect metallographic methods, since the content of almost all impurities after two runs is beyond the detection of the analytical methods. Fractographic tests show that after two runs all the samples have the mixed fracture with a predominance of the transgranular fracture. Samples of one run have the intergranular fracture behavior and on fracture surfaces are observed precipitates (carbides). Cast ingots of undoped high-purity molybdenum of all five runs are plastically deformed by high-temperature pressing using the standard technological scheme adopted for ingots of doped molybdenum. The processing cycle includes heating to 1300^0C in vacuum, hot pressing at the high-speed press with a force of 670 tons, recrystallization annealing in a hydrogen atmosphere at 1300^0C, hot ($900–1300^0$C) and warm (up to 300^0C) rolling. Processing ingots by two to five runs is held normally, without cracking. On ingots of unalloyed high-purity molybdenum of the single run at the stage of hot pressing the cracks appear. The deformation degree is 75–82 %, and the recrystallization annealing temperature is adjusted so that it is possible to obtain a semi-integrated rolling feed with the uniform grains because unalloyed molybdenum has the low recrystallization temperature of about 1000°C (Table 10). The tensile strength of annealed ribbons of undoped high-purity molybdenum is 72 kg mm^{-2},

the elongation of 15.7%. Processing cast ingots of undoped high-purity molybdenum produced by EBM show its high adaptability, which is almost entirely dependent on its purity and lack of large and elongated columnar grains with a poor cohesion. The high technological plasticity of undoped high-purity molybdenum allow producing workpieces of rectangular form or flat bars for deformation processing, cut from cylindrical ingots or melted with a special "flat" mold. Hot-rolling flat bars to a sheet with a thickness of 6.5 mm is similar to the procedure adopted for rolling pressed billets. The use of the flat ingots of undoped high-purity molybdenum allows to eliminate one of the deformation runs and avoid the uncontrolled contamination of the metal and metal losses arising in the preparation of feeds for pressing and rolling. During the duplex process ingots of undoped high-purity molybdenum of the single EBM run are melted in the VAM set-up (vacuum, argon) with a consumable electrode and electromagnetic stirring of the melt. In this case, the consumable electrode is an ingot of high-purity unalloyed molybdenum of the smaller diameter (60 mm) produced by EBM in the EMO-250 set-up (250 kW, axial electron gun, vacuum). The run is carried out with a rate of 2–3 kg/min, with stirring the melt by electromagnetic field of the solenoid. At currents of 1–1.4 A at the solenoid the macrostructure is characterized by grains of up to 60 mm with an average grain size across the eye ~4 mm. At stirring currents up to 5 A the grains lengths are decreased to 15–20 mm, and the average grain size in diameter is 2 mm. The parameters of the electric arc remains constant during the whole run. According to the microstructural analysis the recrystallization of undoped highly pure molybdenum occurs in the temperature range 900–1100⁰C. The results of the mechanical testing of sheet samples of undoped high-purity molybdenum of EBM+VAM have a quite satisfactory performance even at low temperatures from -192⁰C up to 200⁰C (Figure 16).
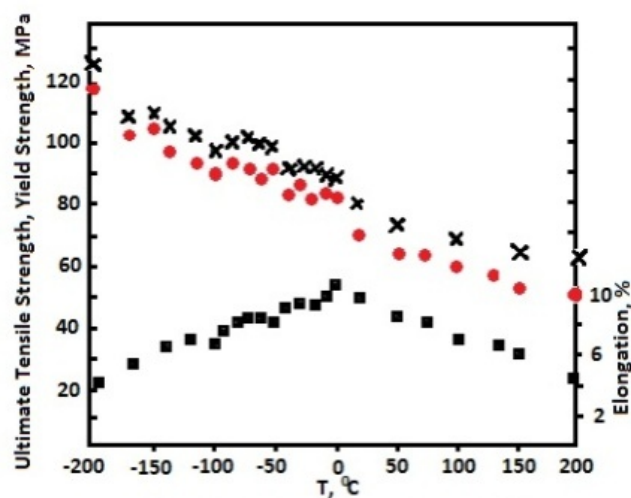

Figure 16. Temperature dependence of the ultimate tensile strength, σ_b (black crosses), yield strength, $\sigma_{0.2}$ (red circles), and elongation, δ (black squares).

3.2. Tungsten

An increase in purity of tungsten can open the possibility of increasing the technological plasticity. Purifying polycrystalline tungsten from gas-forming interstitials, especially oxygen

and carbon, is considered as one of the most effective ways to improve its ductility. The vacuum melting techniques such as electron-beam vacuum melting and electric arc vacuum melting give additional excellent possibilities (especially, refractory metals of high purity) to produce many tungsten products of the higher quality compared with powder metallurgy (PM) products [63-65]. However, in the case of tungsten, the high purity alone cannot give poly-crystalline tungsten ingots of sufficient technological ductility. The defects, such as voids, second-phase inclusions, PM-fragments, and inhomogeneous coarse-grained structures, are only the part of the problem that should be solved before any technology could be recommended for vacuum melting, pressing, extrusion, and rolling the thin sheets and other tungsten products. Apart of this, during plastic deformation and other thermal treatments the contamination of tungsten with hydrogen and oxygen is quite possible, which can introduce different negative effects. This research is devoted to the study of an influence of some structural defects on the plasticity of the high-purity tungsten ingots [63–65]. The tungsten ingots are produced from the relatively pure PM feeds by double vacuum melting consisting of the electron beam melting (the first run) and electric arc-vacuum melting (the second run) with the intensive electromagnetic mixing of the melt. As can be seen from Table 11, tungsten is purified mainly at the first EB-run. The second arc-vacuum melting is important for a better structure homogeneity and the decreasing the tungsten ingot porosity. It seems that the structural quality and the technological plasticity of the tungsten ingots could be improved by studying the melting and plastic deformation processes. The technology is developed for obtaining cast tungsten ingots and their subsequent pressing and rolling.

	Mo	O	C	Si	Ti	P	S	Al	N	Co	Fe
PM rods	50	30	20	10	10	20	10	10	5	2	2
Single run	50	0.5	10	0.2	0.3	0.05	0.05	0.1	0.9	0.03	0.1
Double run	50	0.5	10	0.2	0.3	0.05	0.05	0.1	0.3	0.03	0.1
	F	Hf	Cr	Ca	Ta	Cl	Mg	B	Ni	Na	K
PM rods	-	1	1	1	1	1	1	1	-	1	1
Single run	0.3	0.3	0.1	0.1	1	0.05	0.03	0.01	0.1	0.03	0.03
Double run	0.3	0.3	0.1	0.1	1	0.05	0.03	0.01	0.1	0.03	0.03

Table 11. Chemical composition of tungsten ingots (1×10^{-4} m%).

The ingots for pressing and extrusion are heated in a HF induction vacuum furnace. Hot pressing and extrusion of the cast polycrystalline tungsten ingots are produced with the relative deformation of 70–78%. Then billets for rolling are heated in a hydrogen furnace with a dew point of hydrogen lower than –30°C. Hot rolling of billets is done in a two-high rolling mill equipped with cast iron rolls of 300 mm in diameter and with a rolling rate of 20 m min^{-1}. The density of tungsten is determined by hydrostatic method. The contents of impurities, especially interstitials, are analyzed by mass spectral, vacuum extraction, and nuclear physical methods. The pores and carbide particles of 1 micron or greater are determined by metallo-

graphic methods. The mechanical grinding and polishing with diamond powders are used to prepare specimens to study the structure. After electropolishing in an electrolyte containing soda, chemical etching is carried out by a specific acidic etchant. To avoid overetching of grain boundaries and pores and crumbling of carbides this technique is optimal. Electron scanning microscopy is used to study the pores at large magnifications. The microanalysis of carbon in the carbide particles is conducted in X-ray microanalyser.

In the ingots of 120 mm in diameter the pores are found in the layers up to a depth of 15 mm from the surface (Figure 17). Exclusions accounted only for ingots of an average density (determined by a specific hydrostatic method) of less than 18.9 g/cm^3 (99% of theoretical density of tungsten), the lower density ingots are unsuitable for further processing and referred as the "low" density ingots. In this case, the pores of 5–100 microns are detected through almost all of the bulk of ingots. In the subsurface layers the pores are up to several millimeters. Ingots with a density higher than 18.9 g cm^{-3} are referred to as the "normal" density ingots and contained pores only in the subsurface layers, but at a greater depth the pores are absent. The density estimates obtained by metallography are in a good agreement with results of a hydrostatic density technique. In high-purity tungsten ingots of double EB melting (double run), the sizes of the peripheral grains are 2–2.5 times bigger than in ingots of tungsten doped with carbon (70 ppm). In the center of ingots of the double run the grains are the largest. Thus, it is revealed that grain sizes in the high-purity tungsten ingots are increased from the peripheral area to the center; however, grain sizes in the tungsten ingot doped with carbon, distribute almost uniformly.
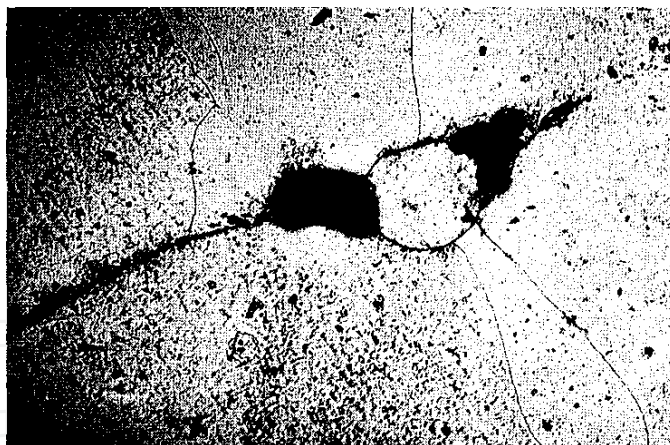

Figure 17. Pores in a tungsten ingot of the "low" density (× 125).

It is found that an absence of pores, cracks, and other structural defects is very important for high-temperature plastic deformation of tungsten. The largest number of defects in the form of pores occurs in the undoped high-purity tungsten ingots of the single EB run, ingots of the double EB run – substantially smaller, ingots of the carbon-doped tungsten produced by the EB-run – the smallest. During the hot plastic deformation of tungsten ingots, the pores change their shape according to the ingot formation. Ingots of undoped high-purity tungsten with highest soundness and technological plasticity are produced by the duplex process consisting

of the EB melted ingots (several electrodes) followed by the run of these ingot-electrodes in the VAM setup with the electromagnetic stirring of the melt. It is much more difficult to observe pores in samples obtained after hot pressing the ingots since as a result of deformation their cross-section size is drastically reduced (Figure 18) and the density of ingots is increased. Among the *bcc* metals tungsten stands out because of its high brittle–ductile transition temperature (usually T_{bd} = 400–600°C). At a temperature below T_{bd} the rolling leads to the brittle fracture of tungsten: for example, the rolling tungsten sheets at 400–600°C should therefore be considered as dangerous. At different stages of the rolling, according the technological regulations, some temperature losses are quite possible. For example, the tungsten sheets should be taken from the hydrogen furnace to the rollers, which usually takes 5–10 s. This procedure leads to typical temperature losses (due to the convective and radiative heat exchange with the ambient medium), which do not exceed 50°C [66]. The tensile strength of pure tungsten above 1100°C is about 300 MPa [67]. Our estimations show that for such a large one-step 60% deformation, the deformation part of the temperature increment is about 70°C. The thermal contact of the hot sheet with the cold rolls should significantly decrease the temperature increase due to deformation. It seems that the most serious temperature decrease occur due to the thermal conduction at the contact between the tungsten sheets and the rolls during rolling.
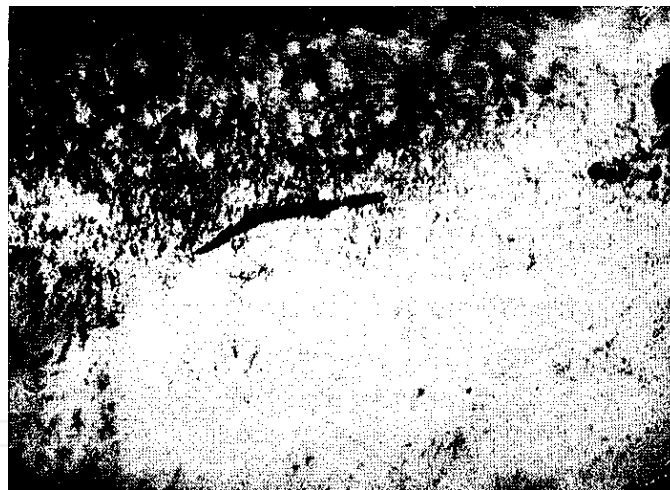

Figure 18. Pores in pressed tungsten prepared from the "low" density tungsten ingot (× 630). The plane is perpendicular to the pressing axis.

A relationship between the sheet thickness and the averaged ΔT is obtained in [68], which allows to estimate the cooling of tungsten billet on the rolls during rolling as a function of the initial temperature (T_w) for a roll temperature, T_r :

$$\Delta T = \frac{4}{H+h}\left(\frac{L}{V_r}\right)^{0.5} \frac{T_w - T_r}{1/a_w^{0.5} + l/a_r^{0.5}\left(c_w\rho_w / c_r\rho_r\right)}$$

where a_r and a_w are the heat conductivities of the cast iron rolls ($1.44 \times 10^{-5} m^2 s^{-1}$) and tungsten at 1400°C ($3.8 \times 10^{-5} m^2 s^{-1}$) respectively. The quantities ρ_w and ρ_r are the densities of tungsten and rolls, c_w and c_r the respective heat capacities, L the length of the deformation site along the rolling direction, V_r the rolling rate, H and h the thicknesses of the sheet before and after rolling respectively. The increase in the length L of the tungsten–rolls contact as compared with $\{R(H-h)\}^{1/2}$ is not taken into account in estimating ΔT. This increase is aroused from elastic flattening of the rolls, especially noticeable during rolling of tungsten. The differences in the heat transfer to the rolls due to formation of the oxide film on tungsten, having an opposite influence on the ingot cooling, are omitted from consideration. Table 12 shows that the temperature losses approach the critical value ΔT=700°C as rolling sheets of 2 mm thick ($H+h = 4\div5$ mm).

Rolling reduction per passage, (H–h) mm	(H+h),mm					
	3	4	5	6	8	10
0.2	643	482	386	321	241	193
0.4	766	574	460	383	287	230
0.6	857	643	514	428	321	257
0.8	904	678	543	452	339	271
1.0	952	714	571	476	357	286

Table 12. Estimation of the mean temperature decrease (°C) on rolling of tungsten heated to 1400°C for different thicknesses of the sheet at the inlet (H) and outlet (h) of the rolling gap

From the technological practice is known that it is at this thickness the tungsten sheets are fractured more often. If an initial microstructure of the tungsten ingots does not guarantee decreasing T_{bd}, the rolling the tungsten sheets below an actual rolling temperature makes them brittle and leads to fracture. It is necessary that the decreasing ductile–brittle transition temperature follows the decreasing rolling temperature as the thickness decreases. So, if T_{bd} would be lower the rolling temperature, the rolling would be still successful: the highly pure tungsten of the "normal" density could be rolled to 1.2–1.5 mm. The sheets from the "low" density tungsten ingots at the same conditions would fracture at 2–4 mm that look like the critical thicknesses. Table 12 demonstrates the mean temperatures at which final passages take place differ by about 200°C. For the "normal" density tungsten ($H+h$) is less than 3 mm whereas for the "low" density tungsten ($H+h$) is more than 4 mm (with reference to initial tungsten ingots).

The temperature T_{bd} of high purity tungsten of the "normal" density is for 200°C lower than that for tungsten of the "low" density ingots. Cracks and voids in fractured tungsten sheets of the "low" density look very different (Figure 19). The specimens for scanning electron microscopy are prepared in the plane perpendicular to the rolling plane. The preparation is done without electropolishing or etching. Thus traces of scratches are even seen in Figure 19 in the direction perpendicular to the rolling. The voids and cracks in the cross-section are

typically of 1–5 microns. It seems as if the cracks are initiated from one point. It should be added that even the rolling is done alternately with anneals, the porosity inherited from the "low" density tungsten ingot could not eliminated. In this respect vacuum-melted tungsten is inferior to that obtained by powder metallurgy. In the latter the small grains and pores of 10 microns in the sheets can be completely sintered of at intermediate anneals. It is absolutely impossible in the coarse-grained vacuum-melted tungsten, which has typical grain sizes of several millimeters. The pores in the "low" density tungsten act like crack nuclei or stress concentrators. To save this possibility, they should be capable before reaching the critical thickness of about 2 mm. Another factor of strengthening and the growth of defects in the "low" density tungsten is hydrogen out of atmosphere of the hydrogen furnace. Hydrogen penetrates very easily into tungsten: The diffusion coefficients (D) of hydrogen are equal to 2 × 10^{-5} to 1.9 × 10^{-4} cm^2 s^{-1} at 900K and 1.6 × 10^{-4} to 2.6 × 10^{-3} cm^2 s^{-1} at 1600 K [69]. After 2 min of heating in the hydrogen furnace, hydrogen penetrates on 0.5 mm at 900 K and 1.4 mm at 1600 K. Hereafter the depth of diffusion is estimated as $(D_\tau)^{1/2}$, corresponding approximately to 50% of the concentration C_0, whereas $2(D_\tau)^{1/2}$ is usually used, corresponding to the lower concen-tration $0.3C_0$. The equilibrium concentration of hydrogen is 3.3 × 10^{-6} at.% at 1200K and 4.0 × 10^{-5} at.% at 1600 K if the hydrogen pressure would be close to 1 atm. As the sheets have been cooled during transportation to the rolling mill or upon rolling, the tungsten becomes oversaturated with hydrogen. Hydrogen travels to the free surfaces and pores, which act as sinks. It is especially pronounced if thickness is less than 5 mm (Table 12, $H+h$ < 10 mm) and the cooling increases dramatically.
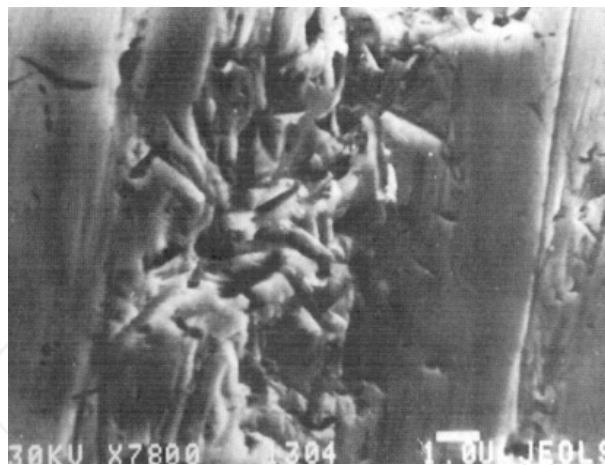

Figure 19. Cracks and pores in hot-rolled sheets of the "low" density tungsten (× 7800). The plane is perpendicular to the rolling direction.

The estimate shows that on cooling for the time period $\tau = 2$ s and starting from the temperature $T_1 = 1400°C$ going to $T_2 = 1200°C$, the equilibrium solubility of hydrogen in tungsten decreases by a value $\Delta c = 4 \times 10^{-5}$ at.%. The characteristic hydrogen diffusion distance during this time is $(D_\tau)^{1/2} \sim 140$ microns (the diffusion coefficient at $T_2 = 1200°C$). At $\alpha \leq 1$ (part of hydrogen), a site of radius $(D_\tau)^{1/2}$ would collect molecular hydrogen in a pore of a volume V_p, thus its pressure would be:

$$p = \frac{\alpha \Delta c 4\pi \left(D\tau \right)^{3/2}}{3\mu_w V_p 2} \rho_w \left(T_2 + 273 \right) R.$$

where μ_w is the tungsten atomic weight, 2 the atoms in the molecule of hydrogen, ρ_w the density of tungsten, and R the gas constant. A pore with a radius of 4 microns and $\alpha = 0.1$, so $p \sim 12$ at. In the case of $\alpha = 1$ and the radius $2(D_r)^{1/2}$ of the site, thus $p \sim 960$ at. It is necessary to know that when the billets or sheets getting smaller during plastic deformation, diffusion, and collection of hydrogen in pores can be fastened. As a result of this process the hydrogen pressure would become much higher than the estimated one. At unloading when the workpiece comes out of rolls, the pressure in pores can be so high that it can be like a source of the explosive initiation and abrupt growth of cracks. The high potential ability of hydrogen to produce significant deformation due to the large and closed pores in tungsten sheets is indirectly confirmed by swelling observed after annealing at 1500°C over and over again (Figure 20). It is the well-known experimental and technological fact: large pores of the initial tungsten ingot are elongated upon rolling and begin to swell. Owing to an increase in pressure and softening of tungsten, the swelling may occur upon heating or resulting from formation of the oversaturated solid solution and collection of hydrogen in pores at temperatures at which tungsten is sufficiently plastic upon cooling. An important feature of the hot rolling of tungsten is the real possibility of the oxygen penetration from surface oxides into the sheets, despite the fact that the sheets are heated before rolling in a reductive hydrogen atmosphere. From our experiments, the average oxygen contents, which can be achieved during technological procedures on tungsten, are usually within $(0.2–5) \times 10^{-4}\%$ with respect to the thickness of the sheets; however, the oxygen contents also depend on the heating temperature and an exposition at which the heated sheets were in air. In this situation the data available concern the diffusion of oxygen in tungsten. It should be noted that tungsten samples (more than 30 samples are examined) with the mean content with respect to thickness higher than $1 \times 10^{-4}\%$ contained cracks formed either upon rolling or during mechanical preparing the specimen for the neutron activation analysis of the oxygen content. We have also studied the carbides distribution in the cast tungsten ingots which is rather non-uniform: at the volumetric carbide content of 0.017–0.055% (the measurements are made using a point technique, several specimens are studied, 25–50 fields of vision, 256 points in each one). There are two different kinds of the porosity defects: areas containing several carbide particles and sites enriched in oxygen. It is found that about 30% of the carbides observed are located at grain boundaries, the remainder being present inside the grains. The carbide particle sizes typically range from 1 to 10 microns. The particles observed are actually carbides, which is supported by two reasons. At first, the microhardness is 13.620 MPa, whereas ones of a tungsten matrix are 4.020–4.120 MPa.

The particles contained larger amounts of carbon as shown by X-ray microanalyser. It is revealed from estimates of a volume fraction of the observed particles that contain carbon satisfactorily agreed with the results of the chemical analysis of carbon. It is shown that carbon contents in the solid solution (carbides) are about $1 \times 10^{-4}\%$ (approximately 10% of the total carbon content).

Figure 20. Swelling of a hot-rolled tungsten sheet from the 'low" density ingot, annealing for 2 h in hydrogen at 1500°C: (a) ingot surface (×2); (b) transverse section, subsurface discontinuities is seen (×80); (c) pore with hydrogen, looks like elongated "bubble" after annealing, splitting cracks are seen (×100).

4. Key findings

1.   A model is proposed within the framework of which specific features of the interaction between interstitials (carbon, oxygen) during high-temperature annealing of refractory metals in vacuum are considered. The limiting carbon concentration that can be attained during a sufficiently prolonged annealing process has been found to depend on the initial carbon/oxygen ratio in the specimen, the specimen geometry, size, and temperature. It has been established that there exists a certain critical concentration of oxygen beginning with which the oxygen effect becomes noticeable and is the more pronounced as the characteristic size of the specimen decreases. A procedure for determining the sticking probability and the effective desorption rate constant for carbon oxide molecules is proposed. The existence of a characteristic critical carbon concentration is shown, above which it can be "burn off" from the metal. The optimal conditions for decarburization annealing of refractory metals (molybdenum, tungsten) are found according to the effective partial pressure of carbon monoxide in the gaseous phase. In a wide range of contents of both interstitials, the kinetics of the interaction processes in liquid niobium, molybdenum, and tungsten in vacuum is studied using the high-frequency levitation and electron-beam zone melting. The direct experimental proofs of the validity of the proposed model and basic predictions are received. The possibility of obtaining refractory metals with the lowest contents of carbon and oxygen is shown: during experiments contents of carbon and oxygen were at the detection limits of activation analysis methods, with the detection limits of the fast neutron activation for oxygen and deuteron activation for carbon being 10^{-5}% and 10^{-6}%, respectively. The regularities and mechanisms of the removal of carbon from the molten niobium, molybdenum, and tungsten at high temperatures in vacuum are studied. The basis is developed on the connection between their satisfactory technological plasticity and the interstitials segregation on grain boundaries. It is also shown that the connection is linear, but rather complicated.

2.   The relationship between the macrostructure and plasticity of molybdenum has been investigated. It is shown that undoped polycrystalline molybdenum of the high purity, produced by multiple electron-beam melting (EBM) or the duplex process consisting

of EBM and vacuum arc melting (VAM) has the satisfactory technological plasticity when subjected to high-temperature processes (pressing, rolling, forging). This feature of this material appears to be connected with the low content of interstitials on the intergranular surfaces and an absence of macrodefects in ingots.

3. The possibility of the refinement of the macrostructure of cast ingots of undoped high-purity molybdenum and tungsten for several times by increasing the melting rate is shown. Efficiency of the technological plasticity at the high-temperature treatment (pressing, rolling) of undoped polycrystalline ingots of molybdenum and tungsten is demonstrated. Unalloyed high-purity molybdenum has the recrystallization temperature of about 1000°C. The recrystallization annealing is used at different stages of the high-temperature processing the undoped high-purity molybdenum and tungsten. Mechanical testing shows that the undoped high-purity molybdenum has the optimistic characteristics of strength and plasticity in the temperature range from -190^0C up to 200^0C, which, at least, are not worse than the standard doped molybdenum alloys.

4. Of the structural factors facilitating brittleness in high-purity polycrystalline tungsten, it is turned out that the most significant factors are (1) the diffusion contamination of the subsurface layers with oxygen and hydrogen (by more than 1×10^{-4}% each with respect to the volume contents) during hot rolling and (2) the decreased density (less than 18.9 g cm^{-3}) of some tungsten ingots. Tungsten ingots of high purity are obtained using vacuum melting techniques. The distribution of pores and carbides in these ingots is investigated. It is found that the cast tungsten ingots with a density of less than 18.9 g cm^{-3} (the "low" density ingots), the sheets produced from these ingots can be fractured under hot rolling. Pores inherited from the initial cast structure facilitate cracking at cooling on the rolls during rolling. It is found that oxygen (more than 10^{-4}%) has a negative influence on tungsten during hot rolling because it has became extremely brittle. At the temperatures lower than the brittle–ductile transition temperature the sheets are fractured. In tungsten of the "low" density, hydrogen is accumulated in pores and cracks while ingots are cooling. This may facilitate brittle fracture of the sheets upon rolling. Within the range of deformation temperatures considered in this study, it is impossible to eliminate the pores inherited from the initial tungsten ingot of the "low" density.

Acknowledgements

Author details

Vadim Glebovsky[*]

Address all correspondence to: glebovs@issp.ac.ru

Institute of Solid State Physics, the Russian Academy of Sciences, Russia

References

[1] Fromm E., Gebhardt E. Gase und Kohlenstoff in Metallen. Berlin. 1976.

[2] Blakely J.M., Shelton J.C. Equilibrium Adsorption and Segregation. In: Surface Physics of Materials, Academic Press; 1975. p100–107.

[3] Seah M.P., Lea C. Surface Segregation and its Relation to Grain Boundary Segregation. Philosophical Magazine 1975;31(3) 627–645.

[4] Lagues M., Domange J.L. Surface Segregation. Comparison between Theory and Experiment. Surface Science 1975; 47 77–85.

[5] Hoffmann S., Erlewein J. A Model of the Kinetics and Equilibria of Surface Segregation in the Monolayer Regime. Surface Science 1978;77 591–602.

[6] Farrel H.H., Isaacs H.S., Strongin M. The Interaction of Oxygen and Nitrogen with the Niobium (100) Surface. II. Reaction Kinetics. Surface Science 1973; 38 31–52.

[7] Pacia H., Dumesic J.A., Weber B., Cassuto A. High Temperature Low Pressure Reactions of Oxygen with Tantalum as Studied by AES and Line-of-sight Mass-spectrometry. Journal of Chemical Society Faraday Transactions 1976;9 1919–1934.

[8] Jupille J., Michel J.M. Desorption d'Oxydes de Niobium a partir de la Solution Solide Niobium-Oxygene, sous 3.10 torr a 3.10 torr d'Oxygen entre 1700 K et 2350 K. Journal of Less-Common Metals 1975;39(1) 17–34.

[9] Gomer R. Chemisorption on Metals. In: Solid State Physics, v.30, New-York-San-Francisco-London: Academic Press; 1975. p94–225.

[10] Muscat J.P., Rewns D.H. Chemisorption on Metals. Progress of Surface Science 1978;9(1) 1–43.

[11] Adamson A.W. Physical Chemistry of Surfaces. 3rd edition, New York: Wiley Interscience. 1980.

[12] Yates J., Madey T. Chemisorption on Rhenium: Nb and CO. Journal of Chemical Physics 1969;51(1) 339–397.

[13] Menzel D. Desorption Phenomena in Topics in Applied Physics. In: Gomer R. (ed.) Interaction on Metal Surfaces. Berlin-Heidelberg-New-York: Springer Verlag. 1975. p102–138.

[14] Weber B., Cassuto A. Elements d'un Modele d'Interactions Oxegene sous Basse Pression - Metaux de Transition a Haute Temperature. Surface Science 1973;39 83–99.

[15] Philippard J.L., Weber B., Cassuto A. Segregation Superficille de Rhenium Induite par l'Oxegene a Travers des Couches Mineces de Platine. Applied Surface Science 1982;10(1) 21–26.

[16] Doyen J., Ertl J. Theory of Carbon Monoxide Chemisorption on Transition Metals. Surface Science 1976;43(1) 197–229.

[17] Fromm E., Gebhardt E. Gase und Kohlenstoff in Metallen. Moscow: Metallurgy, 1980.

[18] Ono K., Moriyama J. Deoxidation of High-melting-point Metals and Alloys in Vacuum. Metallurgical Transactions B 1982;13(1–4) 241–249.

[19] Kulikov I.S. Deoxidation of Metals. Moscow: Metallurgy. 1975.

[20] Gillet E., Chiarena J.C., Gillet M. Decomposition Thermique du Monoxyde de Carbon sur une Surface de Molybdene: Formation de couches Superficielles de Carbon et de Carbure. Surface Science 1976;55 126–140.

[21] Ford R.R. Carbon Monoxide Adsorption on Transition Metals. In: Advances in Catalysis. New-York: Academic Press; 1970.

[22] Jayamatha K., Srinivasan A., Negbe M.S. Interactions of CO with Transition Metal Surfaces. Surface Science 1980;99(2) 309–319.

[23] Jupille J., Cassuto A. Interaction de l'Oxegene aux Basses Pressions avec la Solution Solid Niobium-Oxygene a Haute Temperature. I. Equilibre de Segregation-Chimisorption. Surface Science 1976;60 177–195.

[24] Goymor C.G., King D.A. Chemisorption of Carbon Monoxide on Tungsten. Journal of Chemical Society Faraday Transactions 1973;4 736–760.

[25] King D.A. Thermal Desorption from Metal Surfaces: a Review. Surface Science, 1975, v.47, p.384–402.

[26] Felter T.E., Estrup P.J. Adsorption of Carbon Monoxide on the Molybdenum (100) Surface. Surface Science 1978;76 464–482.

[27] Guillot G., Riwan R., Lecante J. Dissociation of CO on Mo(100). Surface Science 1976;59 581–592.

[28] Klein R., Leder L.B. Field-emission of CO on Tantalum. Journal of Chemical Physics 1963;38(8) 1866–1872.

[29] Gasser R.P.H., Thwaites R. Interaction of Carbon Monoxide with Tantalum. Transactions of Faraday Society 1965;65 2036–2043.

[30] Belov V.D., Ustinov Y.K., Komar A.P. Carbon Monoxide and Carbon Dioxide Interaction with Tantalum. Surface Science 1978;72 390–404.

[31] Ko S.M., Schmidt L.D. Adsorption and Solution of H_2, D_2, N_2, 0_2 and CO by (100)Ta. Surface Science 1975;47 557–568.

[32] Ustinov Y.K. On Determination of Parameters of Diffusion of Adsorbate in Metal Adsorbent by Flashing. Journal of Technical Physics 1972;42 2153–2157.

[33] Kosina L.N., Revyakin A.V., Samarin A.M. Thermodynamic Analysis of Deoxidation of Liquid Molybdenum. Reports of AN 1970;190(4) 909–910.

[34] Kosina L.N., Revyakin A.V., Samarin A.M. About Solubility of Oxygen in Liquid Molybdenum. Russian Metallurgy (Metalli) 1970;1 56–62.

[35] Kosina L.N. Deoxidation Ability of Carbon in Liquid Molybdenum. Russian Metallurgy (Metalli) 1970;2 116–118.

[36] Revyakin A.V., Kuznetsov L.V. Kinetics of Interaction of carbon and Oxygen in Liquid Metals in Vacuum. Russian Metallurgy (Metall) 1973;1 23–29.

[37] Kosina L.N., Revyakin A.V. Analysis of Deoxidation of Liquid Niobium. Russian Metallurgy (Metall) 1975;4 24–26.

[38] Efimov V.E. Kinetics and Mechanism of Interaction of Carbon and Oxygen in Liquid Refractory Metals. Russian Metallurgy (Metalli) 1975;4 27–34.

[39] Efimov V.E. Mechanisms of Interaction and Limiting Concentrations of Interstitials in Molybdenum. Russian Metallurgy (Metalli) 1977;1 39–45.

[40] Efimov V.E. About Interaction of Interstitialas with Metals during Vacuum Refining. Russian Metallurgy (Metalli) 1983;6 38–46.

[41] Efimov V.E. On the Kinetic and Mechanisms of Vacuum Refining Metals of Interstitials. In: Burkhanov G.S. (ed.); Physical and Chemical Basis of Vacuum Processing in Metallurgy. Moscow: Nauka; 1984. p36–42.

[42] Schulze K.K. Preparation and Characterization of Ultra-high Purity Niobium. Journal of Metals 1981;33(5) 33–41.

[43] Reed R.E. Electron-beam Float Zone Melting and Vacuum Degassing of Niobium Single Crystals. Journal of Vacuum Science & Technology 1972;9(6) 1413–1418.

[44] Meyerhogg R.W. Preparation and Electrical Resistivity of Ultrahigh Purity Niobium. Journal of Electrochemical Society 1971;118(6) 997–1001.

[45] Reed R.E. Redistribution of Ta and W Impurities in Niobium by Electron Beam Zone Melting. Journal of Crystal Growth 1973;19 61–67.

[46] Shipilevsky B.M., Glebovsky V.G. The interaction of carbon and oxygen in refractory metals at high temperatures. In: International Conference on High Purity Materials in Science and Technology. Dresden. 1980.

[47] Shipilevsky B.M., Glebovsky V.G. Competition of Bulk And Surface Processes in the Kinetics of Hydrogen and Nitrogen Evolution from Metals into Vacuum. Surface Science 1989;216 509–527.

[48] Shipilevsky B.M., Glebovsky V.G. The Laws of Interaction of Carbon and Oxygen Impurities at High Temperature Annealing of Refractory Metals in Vacuum. Poverkhnost (Surface) 1982;7 26–37.

[49] Shipilevsky B.M., Glebovsky V.G. The Features of Carbon Behavior in Refractory Metals at High-Temperature Annealing in Vacuum. Poverkhnost (Surface) 1982;8 115–119.

[50] Shipilevsky B.M., Glebovsky V.G. Characteristic Features of Interaction between Carbon and Oxygen Impurities during High-temperature Annealing of Refractory Metals in Vacuum. Physics, Chemistry & Mechanics of Surfaces 1982;1(7) 1940–1964.

[51] Shipilevsky B.M., Glebovsky V.G. Features of Carbon Behavior during High-temperature Annealing of Refractory Metals in Vacuum. Physics, Chemistry & Mechanics of Surfaces 1982;1(8) 2291–2310.

[52] Shipilevsky B.M., Glebovsky V.G. Competition of the Bulk and Surface Processes in the Kinetics of Hydrogen and Nitrogen Release from Metals into Vacuum. Vacuum 1990;41 126–129.

[53] Glebovsky V.G., Kapchenko I.V., Shipilevsky B.M. Kinetics of Interaction of Carbon and Oxygen in Niobium during Vacuum Levitation Melting. Journal of Alloys and Compounds 1992;184 305–313.

[54] Kapchenko I.V., Glebovsky V.G., Kireyko V.V., Ryzhkov V.A. Kinetics of Removal of Oxygen and Carbon from Molybdenum during High-frequency Levitation in Vacuum. Vysokochistye Veschestva (High-Purity Materials) 1989; 114–124.

[55] Glebovsky V.G., Shipilevsky B.M., Kapchenko I.V., Kyreiko V.V. Kinetics of Oxygen and Carbon Removal from Liquid Molybdenum in the Process of High-frequency Levitation in Vacuum. Journal of Alloys and Compounds 1992;184 297–304.

[56] Aritomi N. Research on the Brittleness of Electron-Beam Melted Molybdenum. Transactions of Japan National Research Institute of Metals 1979;21 18–34.

[57] Morito F. Intergranular Fracture Surface Analysis of Molybdenum. Surface & Interface Analysis 1990;15 427–432.

[58] Kishore R., Kumar A. Effect of Carbon on Ductilization of Electron-beam Welds in Molybdenum. Journal of Nuclear Materials 1981;101 16–27.

[59] Glebovsky V.G., Kasyanov V.G., Kapchenko I.V., Podvigin V.S. Macrostructure and Plasticity of Molybdenum. High Temperatures-High Pressures 1986;18 453–458.

[60] Glebovsky V.G., Karpov M.I., Kasyanov V.G., Kokhanchik L.S., Medved N.V. Technological Plasticity of Unalloyed Polycrystalline EB-melted Molybdenum. T-00615. Chernogolovka: Institute of Solid State Physics; 1985.

[61] Glebovsky V.G., Kapchenko I.V., Kosachev L.S., Leitman M.S., Podvigin V.N. Effect of some Melting Parameters on Structure and Properties of Unalloyed Molybdenum. In: Burkhanov G.S. (ed.), Study of Refractory Materials: Proceedings of the National Conference for Refractory Metals. Moscow: Nauka Publishers; 1988.

[62] Glebovsky V.G., Karpov M.I., Kasyanov V.G., Kokhanchik L.S., Medved N.V. Macrostructure and Technological Ductility of Unalloyed Molybdenum Produced by Electron Beam Melting. Russian Metallurgy (Metalli) 1986; 112–116.

[63] Gnesin B.A., Glebovsky V.G., Karpov M.I., Kireyko V.V., Snegirev A.A. Some Structural Sources of Brittleness in Cast Tungsten. Journal of Less-Common Metals 1990;167 11–19.

[64] Gnesin B.A., Glebovsky V.G., Karpov M.I., Kireyko V.V., Snegirev A.A. Structural Sources of Brittleness of High-purity Polycrystalline Tungsten. Vysokochistye Veschestva (High-Purity Materials) 1991; 199–203.

[65] Glebovsky V.G., Kapchenko I.V., Kosachev L.S., Egorkin M.I. Structural Sources of Fragility of Tungsten Melted in Vacuum. Burkhanov G.S. (ed.), Proceedings of National Conference on Refractory Metals. Suzdal: Informelectro. 1987.

[66] Medvedev G. A., Denisov P. I., Medvedev A. G. The Method of Metal Temperature Evaluation at Hot Rolling of Sheets and Strips. Sverdlovsk: UPI, 1981.

[67] Kopecky C.V. Structure and Properties of Refractory Metals. Moscow: Metallurgy, 1974.

[68] Novikov I.I., Klimov K.M, Burkhanov Yu.S. About Estimation of Temperature at Hot Rolling. Russian Metallurgy (Metalli) 1983;2 88–92.

[69] Gmelins Handbuch der Anorganischen Chemie, N54 W; Teil Bl. Berlin: Springer Verlag. 1979.